NANOSCIENCE AND TECHNOLOGY: AN INTERNATIONAL JOURNAL

ISSN Print: 2572-4258; ISSN Online: 2572-4266

Publisher- Begell House, USA.

Accepted August 1st 2018

NUMERICAL SIMULATION OF TIME-DEPENDENT NON-NEWTONIAN NANO-PHARMACODYNAMIC TRANSPORT PHENOMENA IN A TAPERED OVERLAPPING STENOSED ARTERY

N. Ali[a], A. Zaman[a], M. Sajid[b], O. Anwar Bég[c], MD. Shamshuddin*[d] and **Ali Kadir[c]**

*[a]Department of Mathematics and Statistics, International Islamic University, Islamabad, 44000, **Pakistan***
*[b]Theoretical Physics Division, PINSTECH, P.O. Nilore, Islamabad, 44000, **Pakistan**.*
*[c]Mechanical/Aeronautical Engineering Department, Newton Building, University of Salford, M5 4WT, **UK**.*
*[d]Department of Mathematics, Vaagdevi College of Engineering, Warangal, Telangana, **India.***
***Emails**: [c]O.A.Beg@salford.ac.uk ; [c] a.kadir@salford.ac.uk.*
Corresponding author: shammaths@gmail.com, mdshamshuddin@vaagdevieng.ac.in

Abstract

Nanofluids are becoming increasingly popular in novel hematological treatments and also advanced nanoscale biomedical devices. Motivated by recent developments in this area, a theoretical and numerical study is described for unsteady pulsatile flow, heat and mass transport through a tapered stenosed artery in the presence of nanoparticles. An appropriate geometric expression is employed to simulate the overlapping stenosed arterial segment. The Sisko non-Newtonian model is employed for hemodynamic rheology. Buongiorno's formulation is employed to model nanoscale effects. The two-dimensional non-linear, coupled equations are simplified for the case of mild stenosis. An explicit forward time central space (**FTCS**) finite difference scheme is employed to obtain a numerical solution of these equations. Validation of the computations is achieved with another numerical method, namely the variational finite element method (**FEM**). The effects of various emerging rheological, nanoscale and thermofluid parameters on flow and heat/mass characteristics of blood are shown via several plots and discussed in detail. The circulating regions inside the flow field are also investigated through instantaneous patterns of streamlines. The work is relevant to nano-pharmacological transport phenomena, a new and exciting area of modern medical fluid dynamics which integrates coupled diffusion, viscous flow and nanoscale drug delivery mechanisms.

Keywords: Pharmacodynamic Simulation: Nanoparticles; Stenosis Hemodynamics; Impedance; Heat and mass transfer; Sisko non-Newtonian fluid; FTCS numerical method; Finite Element Method.

1. INTRODUCTION

The analysis of blood flow through diseased arteries is an important area of bioengineering research which has attracted increasing attention in recent years with developments in computational tools and improved clinical data for mathematical models. The most common arterial ailment is *atherosclerosis*, in which plaque builds up inside the arterial wall. The narrowing of arterial lumen caused by such plaque (which reduces the space of lumen) is usually called *stenosis*. Essentially a stenosis is a condition where an artery wall thickens as a result of fatty materials such as cholesterol. It is quite apparent that development of stenosis in an artery results in the reduction of the blood flow rate or *ischemia*. In the coronary artery, ischemia may cause myocardial infarction while the same process in an artery to the brain can lead to a stroke. Hemodynamic studies reveal that the development of plaques in vessels causes sporadic blood flow rate, boundary layer detachment and high arterial wall shear stress. An excellent review of studies up to the late 1990s has been given by Ku (1997) in which turbulence, energy losses and other aspects are covered. Moreover, the modified hemodynamics in the neighborhood of a gentle stenosis may result in the formation of another stenosis. The combination of two stenosis to form an overlapped stenosed arterial segment can increase vulnerability to ruptures in contrast to a single stenotic arterial segment because of increased wall shear stress and strong recirculating zones. Numerous, theoretical studies, based on the principles of fluid dynamics, are available in the medical engineering literature which address blood flow through overlapping stenosis. Excellent reviews of recent progress in general cardio-vascular applications and specific cerebral applications, respectively, have been provided by Sforza et al. (2009), Duraiswamy et al. (2007) respectively. Chakravarty and Mandal (1994) studied blood flow through an overlapping arterial stenosis, observing that flow velocity diminishes downstream from its value at the onset of the stenosis and further increases upstream towards the overlapping region. Many experimental,

theoretical and numerical studies of specific aspects stenotic flows have also been reported. Pinto et al. (2012) used ANSYS FLUENT computational finite volume software to investigate the hemodynamics of a bifurcating channel with stenosis, as a simulation of the left coronary artery. Both a moderate stenosis (65% of occlusion) and a severe stenosis (90% of occlusion) were considered and it was demonstrated that in the severe case, higher static pressure drop is achieved with a larger deviation between mass flow rates in both branches of the bifurcation accompanied with small recirculation zones downstream of the stenosis region. Karri and Vlachos (2010) measured the influence of phase angle between pressure and flow waveforms for stenosed compliant vessels in coronary and peripheral flows using time resolved digital particle image velocimetry, and provided data for Reynolds numbers of 250, 350, and 450 and corresponding Womersley parameters of 2.7, 3.2, and 3.7. They also determined wall-shear stresses (WSSs), oscillatory shear index (OSI), and recirculation lengths for different stenosed cases. Further studies have been reported in Yap et al. (2010); Boyd et al. (2005); Qiao and Zhang (2014); Chakravarty and Mandal (2000); Maleki et al. (2014); Riahi et al. (2011); Haghighi et al. (2015); Mekheimer and Elkot (2012); Hung and Tsai (1996).

The above studies while categorically establishing the great sensitivity of hemodynamic arterial flows to stenotic geometry, were however all confined to *Newtonian* (Navier-Stokes viscous) flow models which are generally valid only for larger vessels. For decades however, it has been firmly established that blood comprises a sophisticated composite suspension of proteins, lipoproteins, ions, white and red blood cells suspended in plasma (water). Erythrocytes alone constitute 40% of blood by volume and owing to the small semi-solid and toroidal geometry of these cells, they result in a non-trivial elevation in blood viscosity of blood – this contributes to the fact that normal human blood is approximately four times more viscous than water by Merrill

et al. (1963). Furthermore, this viscosity varies in the human circulation system and assumes very strong rheological properties in the microcirculatory system as predicted theoretically and confirmed experimentally by Chien et al. (1984). Moreover, strongly non-Newtonian characteristics are observed in small branches and capillary sections of the body wherein *cell-free skimming* leads to a decrease in viscosity. Hemo-rheology of blood is in all these cases significant, largely due to the shear-dependent viscous properties caused by the non-homogeneous nature of blood at the micro scale. It is therefore essential to modify *Newtonian flow models* to *non-Newtonian models* to simulate correctly the dynamics of blood flow in smaller vessels. This has stimulated significant interest in transferring rheological theories developed in chemical engineering to hemodynamics, in particular in the past two decades. Many different constitutive models have been explored with varying degrees of success. In this regard Ikbal et al. (2012) applied both a power-law and a viscoelastic Oldroyd-B model to analyse hemodynamics, Ramana Reddy and Srikanth (2015) addressed slip flow of blood through a catheterized overlapping artery using Eringen's micropolar model and the Carreau rheological model was implemented by Ali et al. (2015) to investigate the pulsatile flow of blood in a catheterized artery for the case of a mild stenosis. Numerous other models and computational techniques have been implemented in stenotic fluid dynamics and the reader is referred to Chakravarty and Datta (1989); Sankar and Lee (2009); Shupti et al. (2015); Razavi et al. (2011); Shaw et al. (2009); Cho and Kensey (1991); Amornsamankul et al. (2006); Jeong and Rhee (2009); Zaman et al. (2015).

In the above investigations, generally only *hydrodynamics* has been considered. Heat and mass transfer, which are also significant features of real blood flows have been ignored. Thus far very few attempts have been made to investigate the collective flow, heat and mass transfer in pulsatile transport in overlapping stenotic arteries. In both non-stenosed and stenosed blood flows,

the significance of both mass transfer by Tarbell (2003) and heat transfer by Chato (1980) is well-established. For example, Tarbell (2003) has identified that interaction of fluid mechanics and mass transfer is fundamental to many aspects of arterial transport and has highlighted four mass transport mechanisms which may contribute to localized atherosclerosis, namely blood phase-controlled hypoxia, leaky endothelial junctions, transient intercellular junction remodeling, and convective clearance of the subendothelial intima and media. The transport of oxygen as a species in hemodynamic mass transfer is fundamental to health. Furthermore, other bio-chemicals and macromolecules such as plasma proteins and lipoproteins which are manufactured within the blood vessel wall are re-located via Fickian mass diffusion. Mass transfer is therefore integral to a proper understanding of circulatory hemodynamics. Chato (1980) has elaborated on the heat-conducting nature of blood which is essential in transporting thermal energy around the circulation system and explains the "warm feeling" accompanying consumption of food where heat is given off as a byproduct in the body. Several researchers have investigated computationally the rheological blood flow and/or heat/mass transfer problem. Bhargava et al. (2007) used variational finite elements, implicit finite differences and a non-Darcy drag force model to simulate biomagnetic hemodynamics and species diffusion as a model of drug delivery (pharmaco-dynamics) in impeded vessels, evaluating in detail the effects of Schmidt number on the transport phenomena. Zhang et al. (2008) utilized a sudden tubular expansion to simulate arterial stenosis and reported both theoretical and laboratory-based results for the effects of mass transfer from the arterial wall to flowing blood, observing that rate of mass transfer is much greater in zones of disturbed flow with a local maximum around the reattachment point where the wall shear rate is zero. Riahi and Garcia, (2013) considered coupled fluid dynamics and heat diffusion in stenosed arteries for dissipative flow and computed blood plasma and red cell velocities, blood pressure force, blood temperature

and the heat flux on the artery at different axial locations of the stenosis. Further studies of heat and/or mass transfer in stenotic flows include Sarifuddin et al. (2009) who considered non-Newtonian properties. Wang (2008) who studied thermal convection in blood flow in narrow vessels (30-1000 mum) with a two-fluid model, Akbar (2014) who employed a Carreau rheological model for coupled heat and mass transfer in tapered stenotic arterial flow and Bég et al. (2008) who analysed biomagnetic microstructural thermal convection in hemodynamic in capillaries containing porous media using a finite element model.

In recent years another significant development in medical engineering has been the application of *nanofluids*. Nanofluids were pioneered by Choi (1995) initially for thermal enhancement in the transport industries (aerospace, automotive) and energy sectors. They comprise base fluids containing nanoparticles which are nanometer-sized particles. The nanoparticles are normally fabricated from metals, oxides, carbides, or carbon nanotubes owing to high thermal conductivities associated with these materials. Normally the conventional base liquids are water, ethylene glycol and oil. Nanofluids achieve demonstrably higher thermal conductivities compared with base liquids alone and significantly enhance heat exchange rate in the base fluid. In a medical engineering context, nanoparticles have been found to achieve exceptional performance in enhancing thermal and mass diffusion properties of for example drugs injected into the blood stream. An excellent perspective of diverse areas of nanofluid deployment in the treatment of neural, pharmacokinetic, diabetic, cancer and other disorders has been recently presented by Boston Scientific corporation, USA Patent, (2007). Harris and Graffagnini (2007) have also identified new potential applications for nanoparticles in for example nanoparticle blood diagnostic systems, asthma sensors, carbon nanotubes in catheters and stents and anti-bacterial treatment for wounds. In neuro-pharmacological hemodynamics, it has been clinically verified that

nanoparticles can easily penetrate the blood brain barrier (BBB) facilitating the introduction of therapeutic agents into the brain by Spuch et al. (2012). Fullstone et al. (2015) have also recently described the exceptional characteristics of nanoparticles (size, shape and surface chemistry) in assisting effective delivery of drugs within cells or tissue (achieved via modulation of immune system interactions, blood clearance profile and interaction with target cells). They have further shown that erythrocytes aid in effective nanoparticle distribution within capillaries. Further investigations endorsing the promise of nanoparticles in hemodynamic diseases include Owens and Peppas (2006); Yoo et al. (2010) the latter with regard to nano-engineering particle morphology and hitchhiking on red blood cells. A number of mathematical fluid dynamic studies have also explored the influence of nanoparticles on transport phenomena in medical engineering including Tripathi and Bég (2014) who examined peristaltic nanofluid drug delivery systems, Nadeem and Ijaz (2015) who studied nanofluid transport in stenosed blood flow and Akbar et al. (2014) who analyzed nano-particle diffusion in tapered stenotic arteries with wall mass flux. Further investigations of nano-particle dynamics in hematological systems include Tan et al. (2012) and Gentile et al. (2008) who considered nanoparticle mass transfer in intra-vascular rheodynamic Casson blood flow with Taylor-Aris dispersion theory.

The present study is devoted to understanding the effects of *nanoparticle diffusion* on characteristics of blood through overlapping stenosed artery. The Sisko rheological model is employed to simulate blood flow by Sisko (1958) and the Buongiorno model Buongiorno (2006) for nanofluid transport. The Buongiorno formulation, which emphasizes Brownian motion and thermophoresis effects, has been successfully deployed in studies as diverse as peristaltic pumping by Bég and Tripathi (2012) and microbial fuel cell bioconvection exploiting micro-organism propulsion by Bég et al. (2015). The model is aimed at elucidating the interactional effects of

nanoparticles and coupled heat, mass and momentum transfer in rheological stenotic blood flow. Representative Reynolds numbers range from 1 (creeping viscous-dominated flow) in small arterioles to approximately 4000 in the largest artery, the aorta. Owing to the focus on smaller vessels, laminar flow is considered for which turbulence effects may be neglected. Both finite difference and finite element solutions for the derived nonlinear boundary value problem are presented, achieving very good agreement. The present study is to the authors' knowledge the first comprehensive computational investigation of simultaneous nano-rheological flow, heat and mass transfer in overlapping stenotic hemodynamics.

2. GEOMETRIC STENOSIS MODEL

Let us consider viscous incompressible rheological blood flow through a tapered overlapping stenotic artery in the presence of nanoparticles. Both heat and mass transfer occur simultaneously and therefore the blood flow is assumed to be heat-conducting and species diffusivity of nano-particles is distinct from the mass diffusivity of the blood. A cylindrical coordinate system is utilized i.e. $(r,\ \theta,\ z)$, where r, z are the radial and axial components respectively. The mathematical equation for the geometry of the overlapping stenosed artery is represented following Ismail et al. (2007) as:

$$R(z)=\begin{cases}\left(\xi^{*}z+a\right)\left(1-\dfrac{64}{10}\eta\left(\dfrac{11}{32}l_0^3\left(z-d\right)-\dfrac{47}{48}l_0^2\left(z-d\right)^2+l_0\left(z-d\right)^3-\dfrac{1}{3}\left(z-d\right)^4\right)\right), & d\le z\le d+\dfrac{3}{2}l_0,\\ \left(\xi^{*}z+a\right), & \textit{otherwise.}\end{cases} \tag{1}$$

In the above expression d represents the length of *non-stenotic* arterial region, a is radius of normal artery, l_0 the length of stenotic region and $\xi^{*}\ \left(=\tan\phi\right)$ the parameter controlling the convergence or divergence of the post-stenotic region. The geometry of a *non-tapered* artery is shown in **Fig. 1 (a)**. The parameter η is defined as in Ismail et al. (2007):

$$\eta = \frac{4\ \delta^*}{a l_0^{\ 4}}, \tag{2}$$

in which δ^* denote the *critical height* of the stenosis appearing at two specific locations i.e.,

$$z = d + \frac{8l_0}{25},\ and\ z = d + \frac{61l_0}{50}. \tag{3}$$

2.1 Mathematical Rheological Nanoparticle Transport Model

Assuming azimuthal symmetry, the flow of blood through the stenosed arterial segment can be treated as unsteady and two-dimensional. Therefore, the velocity, temperature and concentration fields are defined as:

$$\begin{aligned} \mathbf{V} &= \left[u(r,z,t), 0, w(r,z,t)\right], \\ T &= T(r,z,t), \\ C &= C(r,z,t), \end{aligned} \tag{4}$$

where u and w are the velocity components along the *radial* and *axial* directions, respectively. The vessel walls are assumed isothermal and thermal dispersion and viscous heating effects are negated. In view of (4), the continuity, momentum, energy and nanoparticle conservation equations may be written by amalgamating the Sisko hemodynamic model of Mekheimer and El Kot (2012) and the Buongiorno nanofluid model by Buongiorno (2006) as follows:

$$\frac{\partial u}{\partial r} + \frac{u}{r} + \frac{\partial w}{\partial z} = 0. \tag{5}$$

$$\rho\left(\frac{\partial u}{\partial t} + u\frac{\partial u}{\partial r} + u\frac{\partial w}{\partial z}\right) = -\frac{\partial p}{\partial r} + \left(\frac{1}{r}\frac{\partial}{\partial r}\left(rS_{rr}\right) + \frac{\partial}{\partial z}\left(S_{rz}\right)\right) \tag{6}$$

$$\rho\left(\frac{\partial w}{\partial t} + u\frac{\partial w}{\partial r} + w\frac{\partial w}{\partial z}\right) = -\frac{\partial p}{\partial z} + \left(\frac{1}{r}\frac{\partial}{\partial r}\left(rS_{rz}\right) + \frac{\partial}{\partial z}\left(S_{zz}\right)\right) + \rho g\alpha_t\left(T - T_1\right) + \rho g\alpha_c\left(C - C_1\right) \tag{7}$$

$$\begin{aligned} \left(\rho c\right)_f\left(\frac{\partial T}{\partial t} + u\frac{\partial T}{\partial r} + w\frac{\partial T}{\partial z}\right) &= k\left(\frac{\partial^2 T}{\partial r^2} + \frac{1}{r}\frac{\partial T}{\partial r} + \frac{\partial^2 T}{\partial z^2}\right) \\ &\quad + \left(\rho c\right)_p\left[\left(D_\beta\left(\frac{\partial C}{\partial r}\frac{\partial T}{\partial r} + \frac{\partial C}{\partial z}\frac{\partial T}{\partial z}\right) + \frac{D_T}{\left(T_w - T_1\right)}\left(\left(\frac{\partial T}{\partial r}\right)^2 + \left(\frac{\partial T}{\partial z}\right)^2\right)\right)\right] \end{aligned} \tag{8}$$

$$\frac{\partial C}{\partial t} + u\frac{\partial C}{\partial r} + w\frac{\partial C}{\partial z} = D_\beta\left(\frac{\partial^2 C}{\partial r^2} + \frac{1}{r}\frac{\partial C}{\partial r} + \frac{\partial^2 C}{\partial z^2}\right) + \frac{D_T}{\left(T_w - T_1\right)}\left(\frac{\partial^2 T}{\partial r^2} + \frac{1}{r}\frac{\partial T}{\partial r} + \frac{\partial^2 T}{\partial z^2}\right), \tag{9}$$

In the above equations ρ is the fluid density, c_p is the specific heat, α_t is the coefficient of thermal expansion, g is the acceleration due to gravity, k is the thermal conductivity, α_c is the coefficient of thermal expansion with nano-concentration, $(\rho c)_p$ describes the effective heat capacity of the nanoparticle material, $(\rho c)_f$ denotes heat capacity of the fluid, D_β is the Brownian diffusion coefficient, T_1 is the blood reference temperature, C_1 is reference nanoparticle concentration, T_w is the arterial wall temperature, D_T as the thermophoretic diffusion coefficient. Now to eliminate the component of extra stress appearing in Eq. (6) and (7), we utilize the constitutive law of a Sisko model which reads Zaman et al. (2015); Yilmaz and Gundogdu (2008):

$$\boldsymbol{S} = \left(\mu_\infty + \mu \left(\Pi^2 \right)^{\frac{n-1}{2}} \right) \boldsymbol{A}_1. \tag{10}$$

In Eqn. (10), μ and μ_∞ are the dynamic and infinite-shear-rate viscosities of blood, respectively, n is the power law index and $\boldsymbol{A}_1$ is the first Rivlin-Ericksen tensor given by:

$$\boldsymbol{A}_1 = \Delta \boldsymbol{V} + \Delta \boldsymbol{V}^T. \tag{11}$$

The second invariant of first Rivlin-Ericksen tensor, Π, is defined as:

$$\Pi = \sqrt{\frac{1}{2} tra\left(\boldsymbol{A}_1^2 \right)}. \tag{12}$$

In view of (4), the constitutive relation (10) yields:

$$S_{rr}=2\left[\mu_{\infty}+\mu\left\{\left[\left[2\left(\left(\left(\frac{\partial u}{\partial r}\right)^{2}+\left(\frac{u}{r}\right)^{2}\right)+\left(\frac{\partial w}{\partial z}\right)^{2}\right)+\left(\frac{\partial u}{\partial z}+\frac{\partial w}{\partial r}\right)^{2}\right]\right]\right\}^{\frac{n-1}{2}}\right]\left(\frac{\partial u}{\partial r}\right), \tag{13}$$

$$S_{zz}=2\left[\mu_{\infty}+\mu\left\{\left[\left[2\left(\left(\left(\frac{\partial u}{\partial r}\right)^{2}+\left(\frac{u}{r}\right)^{2}\right)+\left(\frac{\partial w}{\partial z}\right)^{2}\right)+\left(\frac{\partial u}{\partial z}+\frac{\partial w}{\partial r}\right)^{2}\right]\right]\right\}^{\frac{n-1}{2}}\right]\left(\frac{\partial w}{\partial z}\right), \tag{14}$$

$$S_{rz}=\left[\mu_{\infty}+\mu\left\{\left[\left[2\left(\left(\left(\frac{\partial u}{\partial r}\right)^{2}+\left(\frac{u}{r}\right)^{2}\right)+\left(\frac{\partial w}{\partial z}\right)^{2}\right)+\left(\frac{\partial u}{\partial z}+\frac{\partial w}{\partial r}\right)^{2}\right]\right]\right\}^{\frac{n-1}{2}}\right]\left(\frac{\partial w}{\partial r}+\frac{\partial u}{\partial z}\right). \tag{15}$$

2.2 Non- dimensionlization of transport model

The problem defined by Eqs. (5) - (9) and (13) - (15) can be made dimensionless by defining

$$\begin{gathered}\bar{r}=\frac{r}{a},\ \bar{w}=\frac{w}{U_0},\ \bar{u}=\frac{l_0 u}{\delta^{*}U_0},\ \bar{t}=\frac{U_0}{a}t,\ \bar{z}=\frac{z}{l_0},\ \bar{R}=\frac{R}{a},\ \bar{p}=\frac{a^2 p}{U_0 l_0 \mu_0},\ \mu_0=\mu\left(\frac{U_0}{a}\right)^{n-1},\ N_b=\frac{\tau D_\beta C_1}{k}\\ \bar{S}_{rz}=\frac{a}{U_0\mu_0}S_{rz},\ \bar{S}_{rr}=\frac{l_0}{U_0\mu_0}S_{rr},\ \bar{S}_{zz}=\frac{l_0}{U_0\mu_0}S_{zz},\ \theta=\frac{T-T_1}{T_w-T_1},\ m=\frac{\mu_\infty}{\mu_0},\ \mathrm{G}_{r_N}=\frac{\rho g a^2}{\mu_0 U_0}\alpha_C C_1,\\ \sigma=\frac{C-C_1}{C_1},\ Le=\frac{\mu_0}{\rho D_\beta},\ P_r=\frac{c_p\mu_0}{k},\ \mathrm{G}_{r_T}=\frac{\rho g a^2}{\mu_0 U_0}\alpha_T\left(T_w-T_1\right),Re=\frac{\rho U_0 a}{\mu_0},N_t=\frac{\tau D_T}{k}\end{gathered} \tag{16}$$

Here $\bar{r}$ is dimensionless radial coordinate, $\bar{w}$ is dimensionless axial velocity, $\bar{t}$ is dimensionless time, $\bar{z}$ is dimensionless axial coordinate, $\bar{R}$ is dimensionless radius, $\bar{p}$ is dimensionless pressure, μ_0 is dimensionless zero shear rate viscosity, N_b is Brownian motion parameter, $\bar{S}_{rz},\bar{S}_{rr},\bar{S}_{zz}$ are dimensionless stress components of the rheological stress tensor, θ is dimensionless blood temperature, m is dimensionless infinite shear rate viscosity, Gr_N the local nanoparticle (species) Grashof number, σ is dimensionless nanoparticle concentration function, Le is the Lewis number, Pr is Prandtl number, Gr_T the local thermal Grashof number, Re is the Reynolds number and N_t is the thermophoresis parameter. The non-dimensional geometric parameters appearing in the terms defined above are stenosis height parameter $\left(\delta=\delta^{*}/a<<1\right)$, and vessel aspect ratio

$\varepsilon = \left(a/l_0\right)$. Also U_0 designates the average velocity of the blood. Introducing the above variables, Eqns. (5) -(9) and (13) - (15) after dropping the bars, now assume the form:

$$\delta\left(\frac{\partial u}{\partial r}+\frac{u}{r}\right)+\frac{\partial w}{\partial z}=0, \tag{17}$$

$$Re\delta\varepsilon^2\left(\frac{\partial u}{\partial t}+\varepsilon Re\left(\delta u\frac{\partial u}{\partial r}+w\frac{\partial u}{\partial z}\right)\right)=-\frac{\partial p}{\partial r}+\varepsilon^2\left(\frac{1}{r}\frac{\partial}{\partial r}\left(rS_{rr}\right)+\frac{\partial}{\partial z}\left(S_{rz}\right)\right), \tag{18}$$

$$Re\frac{\partial w}{\partial t}+Re\left(\delta\varepsilon u\frac{\partial w}{\partial r}+\varepsilon^2 w\frac{\partial w}{\partial z}\right)=-\frac{\partial p}{\partial z}+\left(\frac{1}{r}\frac{\partial}{\partial r}\left(rS_{rz}\right)+\varepsilon^2\frac{\partial}{\partial z}\left(S_{zz}\right)\right)+\mathrm{Gr}_T\theta+\mathrm{Gr}_N\sigma, \tag{19}$$

$$\begin{aligned}RePr\left(\frac{\partial\theta}{\partial t}+\varepsilon\left(\delta u\frac{\partial\theta}{\partial r}+w\frac{\partial\theta}{\partial z}\right)\right)&=\left(\frac{\partial^2\theta}{\partial r^2}+\frac{1}{r}\frac{\partial\theta}{\partial r}+\varepsilon^2\frac{\partial^2\theta}{\partial z^2}\right)+N_b\left(\frac{\partial\sigma}{\partial r}\frac{\partial\theta}{\partial r}+\varepsilon^2\frac{\partial\sigma}{\partial z}\frac{\partial\theta}{\partial z}\right)\\&\quad+N_t\left(\left(\frac{\partial\theta}{\partial r}\right)^2+\varepsilon^2\left(\frac{\partial\theta}{\partial z}\right)^2\right),\end{aligned} \tag{20}$$

$$Re\ Le\left(\frac{\partial\sigma}{\partial t}+\delta\varepsilon u\frac{\partial\sigma}{\partial r}+\varepsilon^2 w\frac{\partial\sigma}{\partial z}\right)=\left(\frac{\partial^2\sigma}{\partial r^2}+\frac{1}{r}\frac{\partial\sigma}{\partial r}+\varepsilon^2\frac{\partial^2\sigma}{\partial z^2}\right)+\frac{N_t}{N_b}\left(\frac{\partial^2\theta}{\partial r^2}+\frac{1}{r}\frac{\partial\theta}{\partial r}+\varepsilon^2\frac{\partial^2\theta}{\partial z^2}\right), \tag{21}$$

$$S_{rz}=\left[m+\left\{\left\|\left[2\left(\delta\varepsilon\left(\left(\frac{\partial u}{\partial r}\right)^2+\left(\frac{u}{r}\right)^2\right)+\varepsilon\left(\frac{\partial w}{\partial z}\right)^2\right)+\left(\delta\frac{\partial u}{\partial z}+\frac{\partial w}{\partial r}\right)^2\right]\right\|\right\}^{\frac{n-1}{2}}\right]\left(\frac{\partial w}{\partial r}+\delta\frac{\partial u}{\partial z}\right),$$

$$S_{rr}=\left[m+\left\{\left\|\left[2\left(\delta\varepsilon\left(\left(\frac{\partial u}{\partial r}\right)^2+\left(\frac{u}{r}\right)^2\right)+\varepsilon\left(\frac{\partial w}{\partial z}\right)^2\right)+\left(\delta\frac{\partial u}{\partial z}+\frac{\partial w}{\partial r}\right)^2\right]\right\|\right\}^{\frac{n-1}{2}}\right]\left(\varepsilon\delta\frac{\partial u}{\partial r}\right),$$

$$S_{zz}=\left[m+\left\{\left\|\left[2\left(\delta\varepsilon\left(\left(\frac{\partial u}{\partial r}\right)^2+\left(\frac{u}{r}\right)^2\right)+\varepsilon\left(\frac{\partial w}{\partial z}\right)^2\right)+\left(\delta\frac{\partial u}{\partial z}+\frac{\partial w}{\partial r}\right)^2\right]\right\|\right\}^{\frac{n-1}{2}}\right]\left(\varepsilon\frac{\partial w}{\partial z}\right). \tag{22}$$

For the subsequent analysis, we shall assume that $\delta << 1$ and $\varepsilon = O(1)$ i.e. the maximum height of the stenosis is small in comparison with the radius of the artery and also that the radius of artery and length of the stenotic region are of *comparable* magnitude. As a consequence of these assumptions, Eqns. (17) - (22) readily contract to:

$$\frac{\partial p}{\partial r} = 0, \tag{23}$$

$$Re\frac{\partial w}{\partial t} = -\frac{\partial p}{\partial z} + \frac{1}{r}\frac{\partial}{\partial r}\left[r\left\{ m + \left(\left| \frac{\partial w}{\partial r} \right| \right)^{n-1} \right\} \frac{\partial w}{\partial r} \right] + \mathrm{Gr}_T \theta + \mathrm{Gr}_N \sigma, \tag{24}$$

$$RePr\frac{\partial \theta}{\partial t} = \left(\frac{\partial^2 \theta}{\partial r^2} + \frac{1}{r}\frac{\partial \theta}{\partial r} \right) + N_b \left(\frac{\partial \theta}{\partial r}\frac{\partial \sigma}{\partial r} \right) + N_t \left(\frac{\partial \theta}{\partial r} \right)^2, \tag{25}$$

$$Re\ Le\frac{\partial \sigma}{\partial t} = \frac{\partial^2 \sigma}{\partial r^2} + \frac{1}{r}\frac{\partial \sigma}{\partial r} + \frac{N_t}{N_b}\left(\frac{\partial^2 \theta}{\partial r^2} + \frac{1}{r}\frac{\partial \theta}{\partial r} \right), \tag{26}$$

Following Burton (1996), we define the axial pressure gradient as:

$$-\frac{\partial p}{\partial z} = A_0 + A_1 cos\left(2\pi\omega_p t\right), \qquad t > 0 \tag{27}$$

where A_0 is the mean pressure gradient and A_1 is the amplitude of the pulsatile component which is responsible for systolic and diastolic pressures. In dimensionless form, Eqn. (27) becomes:

$$-\frac{\partial p}{\partial z} = B_1\left(1 + e\ cos(c_1 t)\right), \tag{28}$$

where

$$e = \frac{A_1}{A_0},\ \mathrm{c}_1 = \frac{a\ \omega_p}{U_0},\ B_1 = \frac{A_0 a^2}{\mu_0 U_0}. \tag{29}$$

Inserting $-\partial p/\partial z$ into the *axial momentum* Eqn. (24), we get:

$$Re\frac{\partial w}{\partial t} = B_1\left(1 + ecos(c_1 t)\right) + \frac{1}{r}\frac{\partial}{\partial r}\left[r\left\{ m + \left(\left| \frac{\partial w}{\partial r} \right| \right)^{n-1} \right\} \frac{\partial w}{\partial r} \right] + \mathrm{Gr}_T \theta + \mathrm{Gr}_N \sigma. \tag{30}$$

Eqns. (25), (26) and (30) are subject to following boundary and initial conditions:

$$w(r,t)\big|_{r=R}=0,\ \left.\frac{\partial w(r,t)}{\partial r}\right|_{r=0}=0,\ w(r,0)=0.0,$$

$$(31)\ \theta(r,t)\big|_{r=R}=1,\ \left.\frac{\partial \theta(r,t)}{\partial r}\right|_{r=0}=0,\ \theta(r,0)=0.0,$$

$$(32)\ \sigma(r,t)\big|_{r=R}=0,\ \left.\frac{\partial \sigma(r,t)}{\partial r}\right|_{r=0}=0,\ \sigma(r,0)=0.0. \qquad (33)$$

The appropriate formulae for volumetric flow rate, wall shear stress *(WSS)* and resistance impedance in the new variables become:

$$Q=\int_0^R wr\,dr, \qquad (34)$$

$$\tau_S=\left(\left\{m+\left(\left|\frac{\partial w}{\partial r}\right|\right)^{n-1}\right\}\frac{\partial w}{\partial r}\right)_{r=R}, \qquad (35)$$

$$\lambda=\frac{\left(\frac{\partial p}{\partial z}\right)}{Q}, \qquad (36)$$

where

$$R(z)=\left(1+\xi\, z\right)\left[1-\frac{64}{10}\eta_1\left(\frac{11}{32}\left(z-\beta\right)-\frac{47}{48}\left(z-\beta\right)^2+\left(z-\beta\right)^3-\frac{1}{3}\left(z-\beta\right)^4\right)\right],\quad \beta\le z\le \beta+\frac{3}{2}, \qquad (37)$$

with $\eta_1=4\delta,\ \delta=\frac{\delta^*}{a},\ \beta=\frac{d}{l_0},\ \xi=\frac{\xi^* l_0}{a}.$

In Eqn. (37), $\xi=\left(\tan\phi\right)$ is termed the *tapering parameter* and ϕ is the *associated taper angle*. The cases $\phi>0$, $\phi=0$, $\phi<0$ correspond to the *converging*, *non-tapered* and *diverging* tapering artery scenarios, respectively. These cases are illustrated in **Fig. 1 (b)**.

Proceeding with the analysis we employ a *radial* coordinate transformation Ling and Atabek (1972):

$$x=\frac{r}{R(z)} \qquad (38)$$

Eqns. (24), (25) and (26) are thereby rendered into the following form:

$$Re\frac{\partial w}{\partial t} = B_1\left(1+ecos(ct)\right) + \frac{1}{xR^2}\frac{\partial}{\partial x}\left[x\left\{ m+\left(\frac{1}{R}\left|\frac{\partial w}{\partial r}\right|\right)^{n-1}\right\}\frac{\partial w}{\partial x}\right] + \mathrm{G}r_T\theta + \mathrm{G}r_N\sigma \tag{39}$$

$$RePr\frac{\partial \theta}{\partial t} = \frac{1}{R^2}\left(\left(\frac{\partial^2\theta}{\partial x^2}+\frac{1}{x}\frac{\partial\theta}{\partial x}\right)+N_b\left(\frac{\partial\theta}{\partial r}\frac{\partial\sigma}{\partial r}\right)+N_t\left(\frac{\partial\theta}{\partial r}\right)^2\right) \tag{40}$$

$$Re\ Le\frac{\partial \sigma}{\partial t} = \frac{1}{R^2}\left(\left(\frac{\partial^2\sigma}{\partial x^2}+\frac{1}{x}\frac{\partial\sigma}{\partial x}\right)+\frac{N_t}{N_b}\left(\frac{\partial^2\theta}{\partial x^2}+\frac{1}{x}\frac{\partial\theta}{\partial x}\right)\right). \tag{41}$$

Similarly, the dimensionless boundary and initial conditions become:

$$\left.\frac{\partial w}{\partial x}\right|_{x=0} = 0, w\Big|_{x=1} = 0,\ \ w|_{t=0} = 0, \tag{42}$$

$$\left.\frac{\partial \theta}{\partial x}\right|_{x=0} = 0, \theta\Big|_{x=1} = 1,\ \ \theta|_{t=0} = 0, \tag{43}$$

$$\left.\frac{\partial \sigma}{\partial x}\right|_{x=0} = 0, \sigma\Big|_{x=1} = 0,\ \ \sigma|_{t=0} = 0. \tag{44}$$

In a similar fashion, the volumetric flow rate, shear stress at the wall and resistance (impedance), respectively assume the form:

$$Q = R^2\left(\int_0^1 w\,x dx\right), \tag{45}$$

$$\tau_s = \frac{1}{R}\left(\left\{ m+\left(\left|\frac{\partial w}{\partial r}\right|\right)^{n-1}\right\}\frac{\partial w}{\partial r}\right)_{x=1}, \tag{46}$$

$$\lambda = \frac{\left(\frac{\partial p}{\partial z}\right)}{Q}. \tag{47}$$

Substituting the dimensionless form of the pressure gradient in Eqn. (47), we can write:

$$\lambda = \frac{B_1\left(1+ecos(2\pi t)\right)}{\left(\int_0^1 w\,x dx\right)R^2(z)}. \tag{48}$$

3. FTCS FINITE DIFFERENCE NUMERICAL SOLUTION

It is difficult if not intractable to derive analytical solutions for the nonlinear Eqns. (39) - (41). Therefore, a suitable numerical method is employed for the solution. This method, which is lucidly detailed in Hoffmann and Chiang (2000) with further examples of medical flow applications in Ali et al. (2015); Zaman et al. (2015) is *forward in time* (FT) and *central in space* (CS). It is therefore frequently designated as the **FTCS** difference algorithm in computational fluid dynamics. We denote w_i^k as the value of w at node x_i, and similarly t_k denotes the k^{th} time instant. In this notation, the finite difference formulation of various partial derivatives is given as:

$$\frac{\partial w}{\partial x} \cong \frac{w_{i+1}^k - w_{i-1}^k}{2\Delta x} = w_x, \tag{49}$$

$$\frac{\partial^2 w}{\partial x^2} \cong \frac{w_{i+1}^k - 2w_i^k + w_{i-1}^k}{(\Delta x)^2} = w_{xx}, \tag{50}$$

and

$$\frac{\partial w}{\partial t} \cong \frac{w_i^{k+1} - w_i^k}{\Delta t}. \tag{51}$$

Using the above formulae for derivatives, Eqns. (39)- (41), are readily reduced to the following form:

$$w_i^{k+1} = w_i^k + \frac{\Delta t}{Re}\left[\left\{B_1\left(1+ecos(ct^k)\right) + \frac{\mathrm{w}_x}{xR^2}\left\{m+\left(|\mathrm{w}_x|\right)^{n-1}\right\}\right\} + \right.$$
$$\left. + \frac{w_x}{R^2}\frac{\partial}{\partial x}\left\{m+\left(|\mathrm{w}_x|\right)^{n-1}\right\} + \frac{1}{R^2}\left(m+\left(|\mathrm{w}_x|\right)^{n-1}\right)w_{xx}\right] + \mathrm{Gr}_T\ \theta_i^k + \mathrm{Gr}_N\ \sigma_i^k, \tag{52}$$

$$\theta_i^{k+1} = \theta_i^k + \frac{\Delta t}{RePrR^2}\left\{\frac{1}{R^2}\left(\theta_{xx} + \frac{1}{x}\theta_x\right) + N_b\left(\theta_x\sigma_x\right) + N_t\left(\theta_x\right)^2\right\}, \tag{53}$$

$$\sigma_i^{k+1} = \sigma_i^k + \frac{\Delta t}{Re\ Le}\left\{\frac{1}{R^2}\left(\sigma_{xx} + \frac{1}{x}\sigma_x\right) + \frac{N_t}{N_b}\left(\theta_{xx} + \frac{1}{x}\theta_x\right)\right\}. \tag{54}$$

The prescribed boundary conditions are given by:

$$
\begin{aligned}
w_i^1 \;&=\; \theta_i^1 \;=\; \sigma_i^1 = 0\,, && at\ t = 0,\\
w_{N+1}^k = w_N^k,\ \theta_{N+1}^k &= \theta_N^k,\ \sigma_{N+1}^k = \sigma_N^k, && at\ x = 0,\\
w_{N+1}^k = \;& \sigma_{N+1}^k = 0,\ \theta_{N+1}^k = 1, && at\ x = 1,
\end{aligned}
\tag{55}
$$

The numerical solution is pursued for *N+1* uniformly discrete points $x_i, (i = 1, 2, \ldots..N+1)$ with a space grid size $\Delta x = 1/N+1$ at the time levels $t_k = (k-1)\Delta t$, where Δt is the small increment in time. At a particular cross-section of the arterial geometry, the simulations are executed for a specific value of temporal and spatial step sizes $\Delta t = \Delta t_1$ and $\Delta x = \Delta x_1$. Indeed, it is anticipated that for this specific choice the numerical values of velocity, temperature or nano-particle species concentration, may not attain convergence. Convergence to the correct solution is assured by choosing lower values of $\Delta t = \Delta t_2 \left(< \Delta t_1\right)$ and $\Delta x = \Delta x_2 \left(< \Delta x_1\right)$ and then comparing the numerical value of velocity (or temperature or nanoparticle species concentration) with the previously obtained values. To obtain the accuracy of the order $\sim 10^{-7}$, we have taken the following step sizes: $\Delta x = 0.025$ and $\Delta t = 0.00001$. Fast convergence and stable solutions are achieved. The FTCS scheme is relatively easy to implement since the values of, for example, the *velocity* i.e. w_i^{k+1} may be updated independently of each other. The entire solution is contained in two loops: an outer loop over all time steps and an inner loop over all interior space nodes. The algorithm behaves more like the solution to a hyperbolic differential equation than a parabolic differential equation. The solutions to the dimensionless transport equations (39)- (41) under conditions (42)- (44) i.e. the initial and boundary conditions are in fact, as pointed out by Burden and Faires (1997) all bounded, decaying functions. Therefore, the magnitude of the solution will decrease from the initial condition to a constant. The FTCS may if proper care is not taken, yield unstable solutions that oscillate and grow if the time step Δt is too large. However, the FTCS scheme is superior in efficiency and compiles swifter than BTCS (Backward Time Centered Space) scheme.

4. FINITE ELEMENT METHOD VALIDATION OF COMPUTATIONS

The nonlinear boundary value problem described by the coupled eqns. (39)- (41) under conditions (42)- (44) has also been solved with a finite element algorithm. Employing numerical integration rather than numerical differentiation, the adaptability of FEM is well documented. Although numerous formulations are available for this numerical method, the variational weak formulation is particularly adept at solving diffusion phenomena in fluid mechanics. Indeed, it has been applied to some degree of success in recent years in a considerable spectrum of biomechanical transport phenomena problems including pulsating rheological hemodynamics by Bég et al. (2012), nanofluid biopolymer enrobing flows by Latiff et al. (2015), biomagnetic hemodynamics in porous media by Hoque et al. (2013) and very recently magnetized nanofluid coating flows by Rana and Bég (2014). The FEM code, Bio flow in Bhargava et al. (2010) has been modified to stenotic hemodynamics with heat and mass transfer. Pressure gradient is re-defined and time conditions (temporal) also re-defined. Following some numerical tests, mesh-independence is confirmed for the present scenario with approximately 500 finite elements. The whole domain is delineated into a set of 500-line elements of equal width, each element being two-noded. Line elements are adequate since only one spatial variable i.e. normalized radial coordinate, (x) is involved. A variational form is derived for each of the transport eqns. (39)- (41) with the lead master variables w, θ, σ. The numerical integration is performed over the artificial finite element domain in terms of the normalized radial coordinate (x_e; x_e+1) using arbitrary test functions (W_1, W_2) which can be viewed as the variation in the master variables, following Reddy (1985). The nonlinear terms in eqns. (39)- (41) are easily accommodated. The finite element form of the variational equations is achieved by appropriate substitutions based on the following approximations for velocity, temperature and nanoparticle species concentration, respectively:

$$w = \sum_{j=1}^{2} w_j \psi_j \; ; \; \theta = \sum_{j=1}^{2} \theta_j \psi_j \; ; \; \sigma = \sum_{j=1}^{2} \sigma_j \psi_j \tag{56}$$

The weighting functions as in Reddy (1985) are:

$$W_1 = W_2 = \psi_i, \quad i = 1,2 \tag{57}$$

The shape (interpolation) functions for a typical line element (x_e, x_{e+1}) in eqn. (57) are prescribed as follows:

$$\psi_1^{(e)} = \frac{x_{e+1} - x}{x_{e+1} - x_e} \; ; \; \psi_2^{(e)} = \frac{x - x_e}{x_{e+1} - x_e}, \; x_e \le x \le x_{e+1} \tag{58}$$

The *matrix-vector* form of the finite element model is then generated. For brevity details are excluded here and the reader is referred to Bég et al. (2012); Hoque et al. (2013); Rana and Bég (2014); Latiff et al. (2015). This system of non-linear algebraic equations produced after assembly of the element equations is linearized by incorporating functions w, θ, σ, which are assumed to be known. Boundary conditions (42)- (44) are also easily set up. Following imposition of the initial (time) and boundary conditions, the matrix system is condensed and solved iteratively with a modified Householder elimination method, maintaining an accuracy of 0.0005. The comparison of finite difference method (FTCS) and finite element method (FEM) solutions is documented in each of **Figures. 2-10** in the next section where the FEM solution is denoted by ◦ and corresponds only to the solid black line (-) case in each figure. Very close correlation is achieved for radial distributions of velocity, temperature and concentration at different values of m (dimensionless infinite-shear-rate viscosity) in **Figures 2-7** for t =0.45 (prescribed time) and furthermore exceptional agreement is also attained in **Figures 7-10** for temporal distributions of flow rate, wall shear stress and impedance function (flow resistance). **Tables 1 and 2** also show the correlation of FTCS and FEM solutions for the temperature and concentration (nano-particle species) gradients and again very good agreement is obtained. Confidence is therefore very high in the present FTCS computations, which furthermore provide a solid benchmark for future

extensions to the present study and experimentation with other non-Newtonian models. Readers are therefore encouraged to refine the present simulations to consider more complex effects including multiple species diffusion (oxygen, protein equations), variable species diffusivity, variable thermal conductivity and elasticity of the blood vessel.

5. RESULTS AND DISCUSSION

In the following section selected graphical results are displayed using the following set of parameters: $d = 0.5,\ l_0 = 1,\ L = 2.25,\ \mathrm{e} = 1,\ n = 0.7,\ \delta = 0.1, B_1 = 4,\ Re = 1.$ It is important to emphasize that this data correlates closely to actual physical conditions in real blood flow. For example, Prandtl number is prescribed a value of 21, following actual clinical data of Charm et al. (1968) based on room temperature conditions. We note in line with Charm et al. (1968) that although the viscosity, specific heat under constant pressure, and indeed the thermal conductivity of any fluid, including blood, are *temperature-dependent*, the composite of these three properties may be kept constant via a fixed Prandtl number. This has been confirmed to give reasonable accuracy in computational blood flow modelling in Yang (1989). Under the low Reynolds number approximation, which is consistent with rheological flow in small capillaries, *Re* is prescribed as unity i.e. viscous and inertial forces are of the same order of magnitude in the regime. Lewis number which quantifies the ratio of thermal to species (nano-particle mass) diffusivity is prescribed unity implying that both heat and nanoparticles diffuse at the same rate in the blood flow. This is based on data from Lightfoot (1974). Geometric data has been prescribed based on numerous computational (and experimental) studies. The primary objective is to analyze the effects of nanoparticle diffusion and haemo-rheology on various characteristics of flowing blood.

Fig. 2 illustrates the dimensionless velocity profiles for different values of *m (dimensionless infinite-shear-rate viscosity)* at a specific location of the arterial segment *z = 0.77* in the stenotic region. This figure indicates that axial velocity of blood is a progressively decreasing function of *m*. This would appear to agree with the nature of more viscous flows in which greater momentum is required to achieve higher velocity. Blood flow deceleration is therefore anticipated for greater viscosity effect. This is however important in achieving many mass transfer functions in real blood flows as elucidated by Tarbell (2003). The implication for nano-particle diffusion is that it also will be encouraged and more effective in trans-membrane operations since a slower blood flow will enable engineered nano-particles to diffuse better across the vessel into the confining walls and beyond. The trends observed in **Fig. 2** indeed concur with numerous other investigations of stenotic rheological hemodynamics including Shaw et al. (2009) for Casson fluids and Cho and Kensey (1991) for many different non-Newtonian multi-parameter models (e.g. Carreau fluids). In the present computations the Sisko rheological power-law index is set as n = 0.7 corresponding to shear thinning blood. The thermal and species Grashof numbers linked to buoyancy-driven convection both have values of 2 implying that both thermal and species buoyancy forces are twice the viscous hydrodynamic force in the regime. These are entirely reasonable for actual transport in clinical blood flows as confirmed in Yang (1989); Lightfoot (1974).

Fig. 3 presents the evolution of dimensionless velocity profiles for different values of N_t and N_b. Figure 3(a) indicates that the value of axial velocity of blood increases with increasing the thermophoresis parameter N_t. On the contrary, the axial velocity of blood decreases with increasing Brownian motion parameter N_b. The thermophoresis and Brownian motion parameters arise in both the heat conservation (energy diffusion) and mass conservation (nano-particle species

diffusion equations), i.e. eqns. (40) and (41). In the former the terms associated with these parameters are all first order radial temperature or concentration gradients i.e. $N_b\left(\frac{\partial\theta}{\partial r}\frac{\partial\sigma}{\partial r}\right)$ and $N_t\left(\frac{\partial\theta}{\partial r}\right)^2$ respectively. $\frac{N_t}{N_b}\left(\frac{\partial^2\theta}{\partial x^2}+\frac{1}{x}\frac{\partial\theta}{\partial x}\right)$. In the latter however, the associated terms are axial temperature and axial concentration gradients, viz $\frac{N_t}{N_b}\left(\frac{\partial^2\theta}{\partial x^2}+\frac{1}{x}\frac{\partial\theta}{\partial x}\right)$. The influence on the velocity field is sustained via coupling between the energy and species eqns. (40, 41) and the thermal buoyancy ($Gr_T\,\theta$) and species buoyancy ($Gr_N\,\sigma$) linear terms in the momentum eqn. (39). Thermal field will clearly exert influence via the former term and species diffusion field via the latter. The value of N_b is intimately linked with the size of nano-particles. Low N_b values correspond to larger nano-particles and vice versa. The concentration of nano-particles in blood flow will be enhanced with larger N_b (high values of smaller nanoparticle concentrations). This will boost the dominance of the conduction heat transfer which opposes the axial momentum diffusion (heat diffuses faster in this case than momentum). The elevation in thermal conductivity will also result in an increase in thermal diffusivity. This effectively decelerates the axial flow. There are many mechanisms which link the nanoparticle presence to thermal conduction and to fluid mechanical phenomena. These include interfacial layers, Brownian motion, clustering of nanoparticles and the convection-type effects at the nanoscale (nano-convection) which is associated with the nature of heat transport. With regard to the last of these mechanisms, Brownian motion of nanoparticles can produce thermal conduction elevation either indirectly via nano-convection of the fluid surrounding individual nanoparticles or directly via movement of nanoparticles which convey thermal energy (heat) i.e. particle to particle direct solid-solid transport of heat. Whichever mechanism is in action, the global effect on axial flow is a deceleration i.e. slowing. This again is

advantageous to the distribution of carriers in nanofluids which can be transported radially more effectively across the vessel wall into the surrounding tissue. The potential for enhanced and targeted drug delivery is very attractive therefore via the deployment of nanofluids. The boost in axial velocity with thermophoresis effect is linked to the nature of nanoparticle migration towards colder zones in the blood flow. Thermophoresis is the physical manifestation of averaged Brownian motion of particles in a fluid, under the action of a steady temperature gradient. After adequate time elapse, the more vigorous molecular impulses in the hotter fluid region compel the re-location of nano-particles towards the colder region, where weaker molecular impulses are present. On a molecular dynamics level, the stochastic Brownian force imparts molecular impulses on nano-particles. In nanofluids, this force is applied to an ensemble of particles and the corresponding thermophoretic velocity is the mean velocity of the ensemble. Stronger thermophoresis therefore encourages species diffusion towards colder zones which further aids the momentum diffusion. Axial acceleration is therefore assisted by increasing thermophoretic effect. It is also noteworthy that axial velocity is maximized at the vessel centerline and vanishes at the extreme radial coordinate which corresponds to the no-slip condition at the vessel walls. The semi-parabolic profile is evident and characteristic of blood flows in small vessels.

The effects of thermal Grashof number (Gr_T) and nanoparticle Grashof number (Gr_N) are shown in **Figs. 4a, b**. The Grashof number Gr_T is the ratio of thermal buoyancy force to the viscous force while the Grashof of number Gr_N is the ratio of nanoparticle (species) buoyancy force to the viscous force. An increase in Gr_T corresponds to progressively stronger thermal buoyancy force. Similarly, greater values of Gr_N imply stronger nanoparticle species buoyancy force generated by concentration differences in nanoparticles. The axial flow of blood accelerates with an increase in either of Gr_T and Gr_N . The assistive nature of dual buoyancy forces to momentum diffusion and

therefore hemodynamic acceleration is therefore clearly demonstrated. Greater temperature and concentration differences therefore can be exploited in generating more vigorous buoyancy forces in flowing blood and this can benefit axial targeting of drugs. In other words, for specific pharmaco-kinetic agents, the drug can be transported faster along the axial direction via thermal and species buoyancy when nano-particles are present compared to when they are absent. This may be beneficial in for example situations where drugs introduced at one arterial location may be aimed at a significant distance away from that location also i.e. so-called remote pharmacodynamics. Researchers Li et al. (2014) have shown that nano-particles may act as engineered carriers for other agents by electrodeposition synthesis. In this way different types of nano-particles e.g. nano-spheres, nano-ellipses or nanorods can be functionalized by attaching DNA plasmids to the nickel segments and attaching transferrin, a cell-targeting protein, to the gold (metallically bio-compatible) segments, using molecular linkages that selectively bind to only one metal and thus impart bio-functionality to the nanorods in a spatially defined manner. There is further scope infact to map supplementary segments to e.g. nanorods, in order to embed extra bio-functionalities (e.g. endosomolytic agents) or specific drugs for blood disease treatment. In order to maximize effects of pharmacological agents, they are designed to interact in a structurally specific way with a protein receptor or influence positively particular physiological processes within the body, as described by Florence and Attwood (1998). This activates a secondary messenger system which engineers a carefully elected and targeted physiological effect. The new wave of nano-drug therapy can improve on existing methodologies by embedding directionality and accelerating with greater confidence the reversal of required modifications during illnesses in the body to assist its return in a more speedy and effective manner back to the homeostatic state. All bodily functions are a result of interactions of various chemicals and nano-drugs are proven to

achieve better performance in interfering advantageously with these processes. The distinction between nano-pharmaco-fluid mechanics (of which the present work is an example) and pharmaco-kinetics, is that the latter totally negates all fluid dynamics and heat transfer aspects and focuses solely on chemical and mass balances, even in the most sophisticated efforts. Pharmacokinetics only describes the relationship between drug dose and the drug receptor and the time course of drug concentration in the body. It addresses drug dynamics by assuming that the concentration that a drug reaches at its site of action is influenced by the rate and extent to which a drug is absorbed, distributed, metabolized and excreted. Pharmaco-kinetics, as practiced by pharmacists and medical scientists, therefore significantly over-simplifies actual physiological transport phenomena in drug conveyance in the blood and can never truly represent the real picture since viscosity, thermos-physics, arterial geometry and indeed the many interactional aspects of these aspects with mass transfer, cannot be simulated with simple pharmaco-kinetic models. The present study may be one of a number of investigations which could lead to a new era in pharmaco-transport modelling. It is sincerely hoped by the authors that the present work stimulates more interest among engineering scientists to engage in this growing area of medical flow simulation.

Fig. 5 illustrates the dimensionless temperature profiles for different values of Prandtl number (Pr) (panel (a)) and thermophoresis parameter (N_t) (panel (b)) at the stenotic throat of the arterial segment. Figure 5 (a) shows the profiles of temperature of blood inside the artery for Pr =14, 21, 25. The Prandtl number is the ratio of momentum diffusivity to the thermal diffusivity. Larger values of Prandtl number correspond to the case of less heat transfer from the boundary to the fluid. Prandtl number is also the product of dynamic viscosity and specific heat capacity divided by the thermal conductivity of the fluid. Although for simplicity we have constrained each of these physical properties of blood to be constant, tentatively a variation in Prandtl number

implies that one or more of these individual properties changes, and indeed variation in clinical testing of blood flows has confirmed this. The reader is referred to the seminal study of Victor and Shah (1976). For example, it is known that thermal conductivity of whole blood at 37˚C (normal body temperature) is 0.492W/mK and thermal diffusivity is 1.19 ×10–7 m^2/s, compared with pure plasma which has at 21˚C, a thermal conductivity of 0.570 W/mK and thermal diffusivity of 1.21 ×10–7 m^2/s. Blood thermal conductivity however varies considerably from one zone to another and indeed body temperature varies depending on illness. Therefore, an approximation must be made for thermal effects in simulation since it is not possible to have location-specific Prandtl numbers. One reason why heat transfer has been included in the present simulations is that thermophysical effects are intimately associated with homeostasis which is the biological mechanism for maintaining temperature equilibrium within a wide range of environments. The circulatory system of mammals maintains homeostasis by the heart and blood vessels working in unison to sustain a healthy blood flow in the entire circulatory system. Although the geometric model we have considered is much simpler than full clinical systems, it is a good first step in understanding thermal (and other) diffusion processes in real blood flows. Of course, upscaling of the model is needed, and this is best achieved via computational fluid dynamics interfaced with MRI scanned models of actual arterial a stenotic geometry, which is a future objective of the authors Weinbaum et al. (1984). As elaborated earlier Prandtl number is inversely proportional to thermal conductivity (for fixed viscosity and specific heat capacity). Greater Prandtl number therefore implies that less heat is conducted in the blood. The trends in Figure 5(a) are evidently consistent with this logic - a decrease in blood temperature is computed with increasing Prandtl number. It is further observed that the temperature is more sensitive to the increase in Prandtl number near the arterial wall (larger dimensional radius) and no significant variation is observed

in temperature in the vicinity of the center (small dimensional radius), where convection effects dominate thermal conduction effects (absence of tissue suppresses the role of thermal conduction in the bulk flow whereas it maximizes the effect at the wall). This has also been observed and reported by many seminal investigations of blood heat transfer including Weinbaum et al. (1984); Chato (1990). These studies specifically addressed thermally significant small vessels and were not focused on major supply blood vessels. They are therefore relevant to the present work which dwells on smaller vessels where rheological effects are important. However, this also raises other issues. The blood viscosity in these vessels will be more temperature-dependent than in larger vessels, and this will also influence Prandtl number. Furthermore, the pulsatile nature of actual blood flow and the interference effects of a stenosis are probably better analyzed using the wave theory of heat conduction and also improved bio-conduction models for the blood vessel walls. With regard to the latter efforts have been made by Ozisik and Tzou (1994) over two decades ago to integrate wave heat conduction with biological heat transfer and more recently by El Sayed and Bég (2014) to consider non-Fourier bioheat transfer in tissue (vessel walls) with thermal relaxation effects. These aspects we hope to consider in future refinements of the present model which is a platform for doing precisely this. Readers are also encouraged to explore these modifications. There is now a strong consensus that in thermo-fluid simulations of blood flows, especially where the focus is thermal treatment (and this includes nano-drug delivery) the classical method of simulating blood flow as a distributed heat source (or sink) incorrectly presumes that the capillary vasculature is the principal location of heat exchange and that the blood flow term is a scalar property. Kotte et al. (1996) have shown that in reality, the blood flow in a tissue usually has a direction from artery to vein passing through the capillary bed and that blood and proximate tissues do not sustain thermal equilibrium when the blood vessel diameter exceeds 500μm and therefore

heat transfer models for tissue and blood in significantly large vessels must be treated individually. However, this modification is not needed for smaller vessels (rheology is important in these geometries) which we have considered, and the present approximations are certainly justifiable. The effect of thermophoresis parameter (N_t) on blood temperature inside the artery is shown in Figure 5(b). No significant quantitative is observed with increasing the values of thermophoresis parameter. The temperature only slightly increases in the vicinity of the arterial wall with increasing thermophoresis parameter. The thermophoretic effect is a species-dominated effect and is linked to nano-particle diffusion. Although this does affect the hydrodynamics of stenotic blood flow, it does not impact substantially significantly on thermal diffusion in such flows. Indeed, clinical studies Dhont et al. (2007) have confirmed that thermophoresis influence is felt primarily in the velocity field in drug delivery, not in thermal fields, and this is attributable to the fact that physically thermophoresis takes place on a different timescale is essentially a diffusion limited transport process. However other studies have shown that via other procedures such as IR-Laser heating in tissue treatment, thermophoretic effects of associated drugs can be elevated with greater time elapse. Thermophoretic mobility as dictated by the nano-species diffusivity requires a very large thermal load to exert any major influence and laser heating therapy achieves this in Wienken et al. (2010). However, in conventional drug injection into the diseased artery it is not expected that thermophoresis will tangibly modify the thermal distribution in flowing blood and our results concur with these observations.

Fig. 6 illustrates the dimensionless concentration profiles or nanoparticle fraction for different values of thermophoresis parameter (N_t) (panel (a)), Brownian motion parameter (N_b) (panel (b)) and Lewis number (L_e) pane (panel (c)) at the stenotic throat of the arterial segment. Panel (a) shows a strong increase in that the concentration profile with the increase of

thermophoresis parameter (N_t), while it demonstrates the opposite trend with increasing Brownian motion parameter (N_b). The observed behavior of nanoparticle fraction profile with increasing Lewis number is quite similar to its corresponding behavior with increasing Brownian motion parameter. It is also interesting to note that in contrast to the observation made through Figures. 6(a) and 6(b), Figure 6(c) show that the dimensionless concentration profile is less sensitive to Lewis number in the vicinity of the arterial wall. This is probably largely attributable to the absence of trans-wall diffusion (it is impermeable) which reduces the influence of species diffusivity. Lewis number embodies the relative role of thermal diffusion to mass (species) diffusion i.e. it simulates the energy diffusion rate relative to the species diffusion rate. Near the centerline of the artery where convective processes are strongest, Lewis number will be influential- significant modifications in the concentration distributions of nanoparticles are observed here. However, with progression away from the bulk flow region (low dimensionless radius) towards the vessel periphery (higher dimensional radius) the convective process will be stifled, and Lewis number will exert a diminished effect. The profiles are observed to converge in the near-wall region testifying to the weak influence of Lewis number here. It is also noteworthy to mention that when Le=1 both the heat and nanoparticles will diffuse at the same rate. When Le >1, a scenario of most relevance in clinical hemodynamics, as emphasized by Lightfoot (1974), thermal diffusivity exceeds the species diffusivity. We further note that for Le > the peak concentration in nanoparticle species is significantly higher further from the artery centerline compared with Le =1. The profiles grow more sharply in this central core zone of the flow for higher Lewis number than they do for lower Lewis number. The implication is that for nano-drugs with lower species diffusivity than blood thermal diffusivity a greater concentration growth is achieved radially than for drugs which have the same diffusivity as flowing blood. We note also that the finite element method (FEM)

computations achieve exceptionally good correlation with the FTCS finite difference computations in all the figures 2-6 for all values of dimensionless radius i.e. across the artery cross-section.

Fig 7-8 illustrate the time series of volumetric flow rate. In Figure 7, the solid line curve corresponds to a specific set of parameters values i.e. $N_t = 0.5$, $N_b = 0.5$, $Gr_T = 2$, $Gr_N = 3$, $n = 0.7$. *The* others three curves in this figure are produced by varying either of N_t, N_b and Gr_N. A comparison of the solid line curve and of the curve with super imposed circles indicates an increase in volumetric flow rate by increasing Gr_T. Similarly, a comparison of solid line curve with that of curve with superimposed squares reveals an increase in volumetric flow rate with increasing thermophoresis parameter. The effects of Grashof number Gr_N on volumetric flow rate are similar to the effects of thermophoresis parameter (see the axial velocity response in figure 3a) i.e. species Grashof number boosts the volumetric flow rate. The trends in both Figures 7 and 8 are consistent with the assistive influence of both Grashof numbers i.e. both thermal and species buoyancy forces on velocity. Acceleration in the flow enhances volumetric flow rate since for a fixed arterial cross section (and therefore dimensionless radius value), the volumetric flow rate, Q, as defined by eqn. (45) is directly proportional to the axial velocity. Conversely the flow rate is found to decrease with increasing Brownian motion parameter. Again, this concurs with the influence of Brownian motion on axial velocity (fig. 3b) where it induces deceleration. Brownian motion will therefore also deplete the volumetric flow rate. In both figures 7 and 8, the flow rate is found to consistently grow with greater elapse of time. The implication in pharmaco-dynamics is that greater transport of nano-scale drugs is achieved as time elapses and this is precisely the objective in targeted drug delivery and also in medical desires to enforce a particular effect over a certain time period rather than instantaneously. The drug may travel faster in the circulatory system to the target zone.

However, the physiological response should be not too traumatic so that it induces adverse effects in Florence and Attwood (1998).

Fig. 9 illustrates the time series of dimensionless wall shear stress (WSS). The solid line displays the WSS profiles for $N_t = 0.5$, $N_b = 0.5$, $\mathrm{Gr_T} = 2$, $\mathrm{Gr_N} = 3$. The remaining curves are produced by varying either theses parameters. It is observed that the wall shear increases with increasing N_t while it follows a converse trend with N_b i.e. it decreases with increasing N_b. Moreover, it is observed that increase in both thermal and nanoparticle species *Grashof numbers* is to increase the wall shear stress (WSS). Again, this follows logically from the observed acceleration in axial flow in figs. 4 and 4b. In eqn. (46), WSS is defined for the non-dimensional case as $\tau_s = \frac{1}{R}\left(\left\{m + \left(\left|\frac{\partial w}{\partial r}\right|\right)^{n-1}\right\}\frac{\partial w}{\partial r}\right)_{x=1}$, and is therefore strongly linked to radial gradient of the axial velocity i.e. i.e. $\partial w / \partial r$. Since greater Brownian motion parameter (N_b) as observed in figure 3b clearly decelerates axial velocity it will also reduce shear stress at the wall. Velocity boundary layer thickness at the arterial contact surface will therefore be increased. The influence of time on wall shear stress is consistent with numerous studies of stenotic flow including for example, the Newtonian model solutions of Hung and Tsai (1996) and non-Newtonian simulations of Razavi et al. (2011). Axial flow is also accelerated with greater time elapse in the stenosed artery and this manifest in a progressive escalation in the WSS magnitudes. We further note that magnitudes of WSS remain positive indicating that back flow (blood flow reversal) never arises. The periodic nature of the profiles in figures 7-9 is linked to the pulsatile nature of the flow i.e. oscillatory effects.

Fig. 10 demonstrates the time evolution of impedance or resistance to flow at the stenotic throat. Again, a similar procedure is followed to compare various curves as adopted previously. It

is found that resistance to flow rate increases with increasing/decreasing the value of N_b/N_t. On the contrary, the thermal Grashof number serves to reduce the impedance. This is associated with the species buoyancy force, which quantifies the density variation that is due to variable volume fraction of nanoparticles. This force helps the nano-particles exert strong convective heat transfer for low concentrations in the presence of the combined effects of thermophoresis and Brownian motion. The magnitude of resistance is also observed to fall with progression in time since as the flow is accelerated (figure. 9 shows the progressive ascent in WSS) this implies a decreased impedance to the flow with greater time elapse. Again, this pattern is similar to other studies reported in the literature.

Finally, in Figure 11 we have depicted the streamlines for blood flow for specified parameters **Fig. 11**. Panel (a) represents the flow pattern for specific values of Gr_T, Gr_N, δ, and ε. This panel confirms the presence of a circulating bolus of blood enclosed by two streamlines in the overlapping stenotic region of the artery. A comparison of this panel with panels (b) and (c) reveals that there is no significant deviation in size and circulation of the trapped bolus of blood by varying either of Gr_T, Gr_N. This shows that the circulating bolus of blood is less sensitive to the change in thermal and nanoparticle Grashof numbers and thereby the associated buoyancy forces. However, it is observed through the comparison of panel (a) with panels (d)-(f) that streamline patterns are however significantly modified with a change in the shape parameters of the stenosis. It is noted that for a *diverging* artery, the outermost streamlines enclosing the circulating bolus merge in the beginning of the overlapping region resulting in flow acceleration over the whole stenosed segment. On the contrary for a converging artery, the outermost streamlines enclosing the circulating bolus merge in the end of the overlapping region resulting in a flow deceleration (back flow) over the whole stenotic region.

6. CONCLUDING REMARKS

A theoretical and numerical study has been conducted to investigate the nanoparticles effects on rheological blood flow, heat and transfer in an overlapping stenotic artery. The constitutive equation based on the Sisko non-Newtonian model has been incorporated in the present analysis to represent the blood rheology. The model is aimed at simulation of the nano-particle drug delivery in stenosed realistic hemodynamics in small vessels of the human circulatory system. A numerical procedure based on a forward time central space (FTCS) finite difference algorithm has been utilized to obtain computational solutions for the unsteady, nonlinear, coupled nonlinear partial differential equation boundary value problem. Validation of solutions for the general model has been attained using a variational finite element method (FEM). The blood axial velocity, volumetric flow rate, temperature and concentration distributions and also arterial wall shear stress (WSS) and hemodynamic impedance have been computed for a wide range of the merging transport phenomena parameters e.g. rheological index, Brownian motion parameter, thermophoresis parameter, thermal and species (nano-particle) Grashof numbers. The key finding of the current study are:

- The blood axial velocity at the stenotic throat increases with increasing thermal Grashof number. On the contrary, axial flow is decelerated with increasing nanoparticle Grashof number.
- The blood axial velocity at the stenotic throat increases with increasing thermophoresis parameter while it is progressively reduced with greater Brownian motion parameter values.
- The nano-particle species concentration at the cross-section corresponding to the stenotic throat is found to increase by increasing thermophoresis parameter. The opposite response is computed by increasing Brownian motion parameter.

- The nano-particle concentration sharply changes in the vicinity of arterial wall and is generally invariant over the remainder of the arterial cross-section.
- The blood temperature is a decreasing function of Prandtl number. However, it is less sensitive to the change in thermophoresis and Brownian motion parameters.
- A reduction in volumetric flow rate at the stenotic throat is caused by increasing the Brownian motion parameters.
- There is no significant deviation in streamlines of flowing blood by increasing both thermal and nanoparticle Grashof numbers.

The study presented, it is envisaged, will stimulate further interest in more realistic pharmaco-dynamic transport modelling for nano-drugs in stenosed arteries. Efforts in this regard are underway and will be communicated imminently.

FUNDING STATEMENT

This research did not receive any specific grant from funding agencies in the public, commercial, or not- for profit sectors.

DECLARATION OF CONFLICTS OF INTEREST

The author(s) declared no potential conflicts of interest with respect to the research, authorship, and/or publication of this article.

ACKNOWLEDGEMENTS

The authors are grateful to the reviewer for his/her excellent comments which have improved the present work.

REFERENCES

Akbar, N.S., Heat and mass transfer effects on Carreau fluid model for blood flow through a tapered artery with a stenosis, *Int. J. Biomath.,* vol. **07**, no.1, pp. 1450004-1-1450004-21, 2014. http://dx.doi.org/10.1142/S1793524514500041.

Akbar, N.S., Rahman, S.U., Ellahi, R. and Nadeem, S., Nano fluid flow in tapering stenosed arteries with permeable walls, *Int. J. Thermal Sci.*, vol. **85**, pp. 54–61, 2014.

Ali, N., Javid, K., Sajid, M. and Bég, O.A., Numerical simulation of peristaltic flow of a biorheological fluid with shear-dependent viscosity in a curved channel, *Comput. Methods Biomech. Biomed. Eng.*, vol. **19**, no. 6, pp. 614-627, 2015.

Ali, N., Zaman, A., Sajid, M., Nietoc, J.J. and Torres, A., Unsteady non-Newtonian blood flow through a tapered overlapping stenosed catheterized vessel, *Math. Biosci.*, vol. **269**, pp. 94–103, 2015.

Amornsamankul, S., Wiwatanapataphe, B., Wu, Y.H. and Lenbury, Y., Effect of non-Newtonian behaviour of blood on pulsatile flows in stenotic arteries, *Int. J. Biomed. Sci.*, vol. **1**, pp. 42-46, 2006.

Bég, O.A. and Tripathi, D., Mathematica simulation of peristaltic pumping with double-diffusive convection in nanofluids: a bio-nano-engineering model, *Proc. IMECHE Part N: J. Nanoengineering and Nanosystems.*, vol. **225,** pp. 99–114, 2012.

Bég, O.A., Bég, T.A., Bhargava, R., Rawat, S. and Tripathi, D., Finite element study of pulsatile magneto-hemodynamic non-Newtonian flow and drug diffusion in a porous medium channel, *J. Mech. Med. Biol.*, vol. **12**, no.4, pp. 1250081.1 – 1250081.26, 2012.

Bég, O.A., Bhargava, R., Rawat, S., Halim, K. and Takhar, H.S., Computational modeling of biomagnetic micropolar blood flow and heat transfer in a two-dimensional non-Darcian porous medium, *Meccanica.*, vol. **43,** pp. 391-410, 2008.

Bég, O.A., Uddin, M.J. and Khan, W.A., Bioconvective non-Newtonian nanofluid transport in porous media containing micro-organisms in a moving free stream, *J. Mech. Med. Biol.*, vol. **15,** pp. 1550071.1-1550071.20, 2015.

Bhargava, R., Rawat, S., Takhar, H.S. and Bég, O.A., Pulsatile magneto-biofluid flow and mass transfer in a non-Darcian porous medium channel, *Mecannica.*, vol. **42**, pp. 247-262, 2007.

Bhargava, R., Sharma, S., Bég, O.A. and Zueco, J., Finite element study of nonlinear two-dimensional deoxygenated biomagnetic micropolar flow, *Commun. Nonlinear Sci. Numer. Simult.*, vol. **15**, pp. 1210-1233, 2010.

Boston Scientific Sci Med Inc., Method of incorporating carbon nanotubes in a medical appliance, a carbon nanotube medical appliance, and a medical appliance coated using a carbon nanotube technology, PCT (WO/2006/052838), *Boston Scientific Sci Med.*, Inc Website, December 2007.

Boyd, J., Buick, J., Cosgrove, J.A. and Stansell, P., Application of the lattice Boltzmann model to simulated stenosis growth in a two-dimensional carotid artery, *Phys. Med. Biol.*, vol. **50**, no. 20, pp. 4783-4796, 2005.

Buongiorno, J., Convective transport in nanofluids, *ASME J. Heat Transfer.*, vol. **128,** no. 3, pp. 240-250, 2006.

Burden, R.L. and Faires, J.D., *Numerical Analysis*. New York: Brooks/Cole Publishing Co, sixth edition, 1997.

Burton, A.C., *Physiology and Biophysics of the Circulation*, Chicago: Introductory Text, Year Book, Medical Publisher, 1966.

Chakravarty, S. and Datta, A., Effects of stenosis on arterial rheology through a mathematical mode, *Math. Comput. Mod.*, vol. **12**, pp. 1601–1612, 1989.

Chakravarty, S. and Mandal, P.K., Mathematical modelling of blood flow through an overlapping arterial stenosis, *Math. Comput. Mod.*, vol. **19**, pp. 59-70, 1994.

Chakravarty, S. and Mandal, P.K., Two-dimensional blood flow through tapered arteries under stenotic conditions, *Int. J. Non-Linear Mech.*, vol. **35**, pp. 779–793, 2000.

Charm, S., Paltiel, B. and Kurland, G.S., Heat transfer coefficients in blood flow, *Biorheology*., vol. **5**, no. 2, pp. 133-45,1968.

Chato, J.C., *Fundamentals of Bioheat Transfer. Thermal Dosimetry and Treatment Planning. Series in Clinical Thermology*, New York: Wiley, pp. 1-56, 1990.

Chato, J.C., Heat transfer to blood vessels, *ASME J. Biomech. Eng.*, vol. **102**, no. 2, pp. 110-118, 1980.

Chien, S., Usami, S. and Skalak, R., *Blood flow in small tubes, in: Handbook of Physiology*, eds. E. Renkins and C.C. Michel, Section 2: The cardiovascular system, Volume IV, Parts 1 and 2: Microcirculation, American Physiological Society, Bethesda, Indiana, pp. 217-249, 1984.

Cho, Y.I. and Kensey, K.R., Effects of non-Newtonian viscosity of blood on flows in a diseased arterial vessel. Part 1: steady flows, *Biorheology.*, vol. **28**, pp. 241–262, 1991.

Choi, S.U.S., Enhancing thermal conductivity of fluid with nanoparticles, in: D.A. Siginer, H.P. Wang (Eds.), Developments and Application of Non- Newtonian Flows, New York: *ASME.*, vol. **66**, pp. 99-105,1995.

Dhont, J.K., Wiegand, S., Duhr, S. and Braun, D., Thermo diffusion of charged colloids: single-particle diffusion, *Langmuir*., vol. **23**, pp. 1674–1683, 2007.

Duriaswamy, N., Schoephoerster, R.T., Moreno, M.R., and Moore, J. E., Jr., Stented artery flow patterns and their effects on the artery wall, *Ann. Rev. Fluid Mech.*, vol. **39**, pp. 357-382, 2007.

Elsayed, A.F. and Bég, O.A., New computational approaches for biophysical heat transfer in tissue under ultrasonic waves: Variational iteration and Chebyshev spectral simulations, *J. Mech. Med. Biol.*, vol. **14**, no. 3, pp. 1450043.1-1450043.17, 2014.

Florence, A.T. and Attwood, D., *Physicochemical Principles of Pharmacy*, UK: Macmillan Press, 3rd edition, 1998.

Fullstone, G., Wood, J., Holcombe, M. and Battaglia, G., Modelling the transport of nanoparticles under blood flow using an agent-based approach, *Nature Scientific Reports.*, vol. **5**, pp. 1-13, 2015.

Gentile, F., Ferrari, M. and Decuzzi, P., The transport of nanoparticles in blood vessels: the effect of vessel permeability and blood rheology, *Ann. Biomed. Eng.*, vol. **36**, no.2, pp. 254-61, 2008.

Haghighi, A.R., Asl, M.S. and Kiyasatfar, M., Mathematical modeling of unsteady blood flow through elastic tapered artery with overlapping stenosis, *J. Braz. Soc. Mech. Sci. Eng.*, vol **37**, pp. 571-578, 2015.

Harris, D.L. and Graffagnini, M.J., Nanomaterials in medical devices: a snapshot of markets, technologies and companies, *Nanotechnology Law & Business: Winter.*, vol. **4**, no.4, pp. 415-422, 2007.

Hoffmann, K.A. and Chiang, S.T., *Computational Fluid Dynamics*, USA: Engineering Edition System, Wichita, 2000.

Hoque, M.M., Alam, M.M., Ferdows, M., Bég, O.A., Numerical simulation of Dean number and curvature effects on magneto-biofluid flow through a curved conduit, *Proc. IMECHE- Part H: J Eng. Med.*, vol. **227**, no. 11, pp. 1155-70, 2013.

Hung, T.K., and Tsai, T., Pulsatile blood flows in stenotic artery, *ASCE J. Eng. Mech.*, vol. **122**, pp. 890-896, 1996.

Ikbal, A.M., Chakravarty, S., Sarifuddin, and Mandal, P.K., Unsteady analysis of viscoelastic blood flow through arterial stenosis, *Chem. Eng. Commun.*, vol. **199**, pp. 40–62, 2012.

Ismail, Z., Abdullah, I., Mustapha, N., Amin, N., A power-law model of blood flow through a tapered overlapping stenosed artery. *Appl. Math. Comput*., vol. **195**, pp. 669–680, 2007.

Jeong, W.W., and Rhee, K., Effects of surface geometry and non-Newtonian viscosity on the flow field in arterial stenosis, *J. Mech. Sci. Tech.*, vol. **23,** pp. 2424-2433, 2009.

Karri, S., and Vlachos, P.P., Time-resolved DPIV investigation of pulsatile flow in symmetric stenotic arteries-effects of phase angle, *ASME J. Biomech. Eng.*, vol. **132**, no. 3, Article ID:031010, 2010.
http://dx.doi.org/10.1115/1.4000934.

Kotte, A., Van Leeuwen, G., de Bree, J., Van der Koijk, J., Crezee, H., and Lagendjik, J., A description of discrete vessel segments in thermal modeling of tissues, *Phys. Med. Biol.*, vol. **41**, pp. 865–84,1996.

Ku, D.N., Blood flow in arteries, *Ann. Rev. Fluid Mech.*, vol. **29**, pp. 399–434, 1997.

Latiff, N.A.A, Uddin, M.J., Bég, O.A., and Ismail, A.I.M., Unsteady forced bioconvection slip flow of a micropolar nanofluid from a stretching/ shrinking sheet, *Proc. IMECHE- Part N: J. Nanoengineering and Nanosystems.*, vol. **230**, no. 4, pp. 177-187, 2015.

Li, S., Zhang, C., Cao, W., Ma, B., Ma, X., Jin, S., Zhang, J., Wang, P.C., Li, F., and Liang, X.J., Anchoring effects of surface chemistry on gold nanorods: modulates autophagy, *J. Mater. Chem. B: Mater. Biol. Med.*, vol. **28**, pp. 3324-3330, 2014.

Lightfoot, E.N., *Transport Phenomena and Living Systems: Biomedical Applications of Momentum and Mass Transfer*, New York: Wiley, 1974.

Ling, S.C., Atabek, H.B., A nonlinear analysis of pulsatile flow in arteries, *J. Fluid Mech.*, vol. **55**, pp. 493–511, 1972.

Maleki, H., Shahriari, S., Labrosse, M., Pibarot, P., and Kadem, L., An in vitro model of aortic stenosis for the assessment of transcatheter aortic valve implantation, *ASME J. Biomech. Eng.*, vol. **136**, no. 5, pp. 054501-1-054501-4, 2014. http://dx.doi.org/10.1115/1.4026576.

Mekheimer, K.S., Elkot, M.A., Mathematical modeling of axial flow between two eccentric cylinders: Application on the injection of eccentric catheter through stenotic arteries, *Int. J. Non-Linear Mech.*, vol. **47**, pp. 927–937, 2012.

Mekheimer, K.S. and El Kot M.A., Mathematical modelling of unsteady flow of a Sisko fluid through an anisotropically tapered elastic arteries with time-variant overlapping stenosis, *Applied Mathematical Modelling*, vol. **36**, pp. 5393-5407, 2012.

Merrill, E.W., Cokelet, G.R., Britten, A., and Wells, R.E., Jr., Non-Newtonian rheology of human blood, *Circulation Res.*, vol. **13**, pp. 48-60, 1963.

Nadeem, S., and Ijaz, S., Theoretical analysis of metallic nanoparticles on blood flow through stenosed artery with permeable walls, *Physics Letters A.*, vol. **379**, pp. 542–554, 2015.

Otsuka, H., Nagasaki, Y., and Kataoka, K., PEGylated nanoparticles for biological and pharmaceutical applications, *Advance Drug Delivery Review.*, vol. **55**, pp. 403–419,2003.

Owens, D.E., and Peppas, N.A., Opsonization, bio-distribution and pharmacokinetics of polymeric nanoparticles, *Int. J. Pharm.*, vol. **307**, pp. 93–102, 2006.

Ozisik, M.N., and Tzou, D.Y., On the wave theory in heat conduction, *ASME J. Heat Transfer*., vol. **116**, pp. 525-536,1994.

Pinto, S.I.S., Costa, E.D., Campos, J.B.L.M., and Miranda, J.M., Study of blood flow in a bifurcation with a stenosis, *15th Int. Conf. Experimental Mech.*, 22-27 July, Porto/Portugal, 2012.

Qiao, A., and Zhang, Z., Numerical simulation of vertebral artery stenosis treated with different stents, *ASME J. Biomech. Eng.*, vol. **136**, no. 4, Article ID:041007, 2014. http://dx.doi.org/10.1115/1.4026229.

Ramana Reddy, J.V., and Srikanth, D., The polar fluid model for blood flow through a tapered artery with overlapping stenosis: effects of catheter and velocity slip, *Appl. Bionics Biomech.*, vol. **2015**, Article ID:174387 (12 pages), 2015. http://dx.doi.org/10.1155/2015/174387.

Rana, P., and Bég, O.A., Mixed convection flow along an inclined permeable plate: effect of magnetic field, nanolayer conductivity and nanoparticle diameter, *Applied Nanoscience*., vol. **5,** no. 5, 569-581, 2014.

Razavi, A., Shirani, E., and Sadeghi, M.R., Numerical simulation of blood pulsatile flow in a stenosed carotid artery using different rheological models, *J. Biomech.*, vol. **44**, pp. 2021–2030, 2011.

Reddy, J.N., *An Introduction to the Finite Element Method*, New York: MacGraw-Hill, 1985.

Riahi, D.N., and Garcia, A.E., Flow and heat transfer in an artery with stenosis, *Proc. 14th Int. Conf. Mathematics and Computers in Biology and Chemistry (MCBC '13)*, Baltimore, September 17-19, Maryland, USA, 2013.

Riahi, D.N., Roy, R., and Cavazos, S., On arterial blood flow in the presence of an overlapping stenosis, *Math. Comp. Mod.*, vol. **54**, pp. 2999-3006, 2011.

Sankar, D.S., and Lee, U., Mathematical modeling of pulsatile flow of non-Newtonian fluid in stenosed arteries, *Commun. Nonlinear Sci. Numer. Simult.*, vol. **14**, pp. 2971–2981, 2009.

Sarifuddin., Chakravarty, S., and Mandal, P.K., Effect of heat and mass transfer on non-Newtonian flow -Links to atherosclerosis, *Int. J. Heat Mass Transfer.*, vol. **52**, pp. 5719-5730, 2009.

Sforza, D.M., Putman, C.M., and Cebral, J.R., Hemodynamics of cerebral aneurysms, *Ann. Rev. Fluid Mech.*, vol. **41**, pp. 91-107, 2009.

Shaw, S., Gorla, R.S.R., Murthy, P.V.S.N., and Ng, C.O., Pulsatile Casson fluid flow through a stenosed bifurcated artery, *Int. J. Fluid Mech. Research.*, vol. **36**, no. 1, 43–63, 2009.

Shupti, S.P., Rabby, M.G., and Molla, M.M., Rheological behaviour of physiological pulsatile flow through a model arterial stenosis with moving wall, *J. Fluids.*, vol. **2015,** Article ID:546716 (22 pages), 2015. http://dx.doi.org/10.1155/2015/546716.

Sisko, A.W., The flow of lubricating greases, *Ind. Eng. Chem.*, vol. **50**, no. 12, pp. 1789–1792,1958.

Spuch, C., Saida, O., and Navarro, C., Advances in the treatment of neurodegenerative disorders employing nanoparticles recent patents on drug delivery & formulation, *Recent Patents on Drug Delivery & Formulation.*, vol. **6**, pp. 2-18, 2012.

Tan, J., Thomas, A., and Liu, Y., Influence of red blood cells on nanoparticle targeted delivery in microcirculation, *Soft Matter.*, vol. **8**, pp. 1934-1946,2012.

Tarbell, J.M., Mass transport in arteries and the localization of atherosclerosis, *Ann. Rev. Biomed. Eng.*, vol. **5**, pp. 79–118, 2003.

Tripathi, D., and Bég, O.A., A study on peristaltic flow of nanofluids: Application in drug delivery systems, *Int. J. Heat Mass Transfer.*, vol. **70**, pp. 61–70,2014.

Victor, S.A., Shah, V.L., Steady state heat transfer to blood flowing in the entrance region of a tube, *Int. J. Heat Mass Transfer.*, vol. **19**, pp. 777-783, 1976.

Wang, C.Y., Heat transfer to blood flow in a small tube, *ASME J. Biomech. Eng.*, vol. **130**, pp. 024501-1-024501-3, 2008.

Weinbaum, S., Jiji, L.M., and Lemons, D.E., Theory and experiment for the effect of vascular temperature on surface tissue heat transfer-part 11: model formulation and solution, *ASME J. Biomech. Eng.*, vol. **106**, no. 4, 331-341, 1984.

Wienken, C.J., Baaske, P., Rothbauer, U., Braun, D., and Duhr, S., Protein binding assays in biological liquids using microscale thermophoresis, *Nat. Commun.*, vol. **1**, pp. 10-15, 2010.

Yang, W.J., *Biothermal Fluid Sciences-Principles and Applications*, USA: Hemisphere, 1989.

Yap, C., Dasi, L.P., Yoganathan, A.P., Dynamic hemodynamic energy loss in normal and stenosed aortic valves. *ASME J. Biomech. Eng.*, vol. **132**, no. 2, pp. 021005-1-021005-10, 2010. http://dx.doi.org/10.1115/1.4000874.

Yilmaz, F., and Gundogdu, M.Y., A critical review on blood flow in large arteries; relevance to blood rheology, viscosity models, and physiologic conditions, *Korea-Australia Rheol J.*, vol. **20**, pp. 197-211, 2008.

Yoo, J.W., Chambers, E., and Mitragotri, S., Factors that control the circulation time of nanoparticles in blood: challenges, solutions and future prospects, *Current Pharmaceutical Design*., vol. **16**, no. 21, 2298-2307,2010.

Zaman, A., Ali, N., and Bég, O.A., Numerical study of unsteady blood flow through a vessel using Sisko model, *Eng. Sci. Tech: An Int. J.*, vol. **19**, no. 1, pp. 538-547, 2015. http://dx.doi.org/10.1016/j.jestch.2015.09.013.

Zaman, A., Ali, N., and Bég, O.A., Unsteady magnetohydrodynamic blood flow in a porous-saturated overlapping stenotic artery: numerical modeling, *J. Mech. Med. Biol.*, vol. **16**, no. 2, pp. 1650049-1-1650049-16, 2015. http://dx.doi.org/10.1142/S0219519416500494.

Zaman, A., Ali, N., Sajid, M., and Hayat, T., Effects of unsteadiness and non-Newtonian rheology on blood flow through a tapered time-variant stenotic artery, *AIP Advances.*, vol. **5**, pp. 037129-1-037129-13, 2015. http://dx.doi.org/10.1063/1.4916043.

Zhang, Z., Deng, X., Fan, Y., and Guidoin, R., The effects of recirculation flows on mass transfer from the arterial wall to flowing blood, *ASAIO J.*, vol. **54**, no. 1, pp. 37-43,2008.

TABLES

TABLE 1: - Temperature gradient at the wall at different axial locations in the stenotic region with $\mathrm{Gr}_T = 2,\ \mathrm{Gr}_N = 3,\ Le = 1,\ N_b = 0.5, \delta = 0.1,\ t = 0.45,\ \mathrm{Re} = 3, B_1 = 4, n = 0.7, m = 0.175, e = 1.$

$\left.\frac{1}{R}\frac{\partial\theta}{\partial x}\right\|_{x=1}$						
z	$Pr = 21, N_t = 0.5$		$Pr = 14$		$N_t = 0.1$	
	FDM	FEM	FDM	FEM	FDM	FEM
0.5500	3.2881	3.2882	2.5749	2.5747	3.3360	3.3361
0.7700	3.2561	3.2563	2.5411	2.5412	3.2939	3.2940
1.0000	3.2657	3.2655	2.5512	2.5513	3.3063	3.3064
1.2600	3.2757	3.2756	2.5618	2.5619	3.3194	3.3195
1.7100	3.2560	3.2561	2.5410	2.5412	3.2938	3.2939
2.0000	3.2972	3.2974	2.5846	2.5848	3.3483	3.3482

TABLE 2: Concentration gradient at the wall at different axial locations in the stenotic region with $\mathrm{Gr}_T = 2,\ \mathrm{Gr}_N = 3,\ Le = 1,\ \delta = 0.1, t = 0.45, \mathrm{Re} = 3, B_1 = 4, n = 0.7, m = 0.175, e = 1.$

$\left.\frac{1}{R}\frac{\partial\sigma}{\partial x}\right\|_{x=1}$								
z	$Pr = 21, N_b = N_t = 0.5$		$Pr = 14$		$N_t = 0.1$		$N_b = 0.1$	
	FDM	FEM	FDM	FEM	FDM	FEM	FDM	FEM
0.5500	-3.3174	-3.3175	-2.6348	-2.6347	-0.6733	-0.6734	-16.5869	-16.5870
0.7700	-3.3256	-3.3257	-2.6407	-2.6408	-0.6730	-0.6731	-16.6281	-16.6282
1.0000	-3.3246	-3.3247	-2.6404	-2.6405	-0.6733	-0.6734	-16.6231	-16.6230
1.2600	-3.3223	-3.3221	-2.6388	-2.6389	-0.6734	-0.6735	-16.6114	-16.6112
1.7100	-3.3256	-3.3255	-2.6407	-2.6408	-0.6730	-0.6732	-16.6281	-16.6280
2.0000	-3.3123	-3.3122	-2.6302	-2.6301	-0.6729	-0.6728	-16.5613	-16.5612

FIGURE CAPTIONS

FIG. 1: Geometry of the overlapping stenotic artery

FIG. 2. Variation of axial velocity for different values of *m* with

$$\mathrm{Gr}_T = 2,\ \mathrm{Gr}_N = 2,\ N_t = N_b = 0.5, Pr = 21,\ t = 0.45.$$

FIG. 3. Variation of axial velocity for different values of $\mathrm{N_t}$ (left) and $\mathrm{N_b}$ (right) with:

$$\mathrm{Gr}_T = 2,\ \mathrm{Gr}_N = 2,\ N_t = N_b = 0.5, Pr = 21,\ t = 0.45.$$

FIG. 4 (a). Variation of axial velocity for different values of Gr_T with the following data*:*

$$N_t = N_b = 0.5,\ m = 0.175, \delta = 0.1,\ \mathrm{Pr} = 21,\ \mathrm{Gr}_T = 2,\ t = 0.45.$$

FIG. 4 (b). Variation of axial velocity for different values of Gr_N with the following data*:*

$$N_t = N_b = 0.5,\ m = 0.175, \delta = 0.1,\ \mathrm{Pr} = 21,\ \mathrm{Gr}_N = 2,\ t = 0.45.$$

FIG. 5 (a). Temperature profile at different values of P_r with the following data*:*

$$\mathrm{Gr}_T = 2,\ \mathrm{Gr}_N = 2,\ N_t = 0.5, \delta = 0.1, t = 0.45.$$

FIG. 5 (b). Temperature profile at different values of N_t with the following data*:*

$$\mathrm{Gr}_T = 2,\ \mathrm{Gr}_N = 2,\ Pr = 21, \delta = 0.1,\ t = 0.45.$$

FIG. 6(a). Concentration of mas profile at different values of N_t with the following data*:*

$$\mathrm{Gr}_T = 2,\ \mathrm{Gr}_N = 2,\ Le = 1,\ N_b = 0.5, \delta = 0.1, \mathrm{Pr} = 21,\ t = 0.45.$$

FIG. 6 (b). Concentration of mas profile at different values of N_b with the following data*:*

$$\mathrm{Gr}_T = 2,\ \mathrm{Gr}_N = 2,\ N_t = 0.5, Le = 1, \delta = 0.1, \mathrm{Pr} = 21,\ t = 0.45.$$

FIG. 6 (c). Concentration of mas profile at different values of *Le* with the following data*:*

$$\mathrm{Gr}_T = 2,\ \mathrm{Gr}_N = 2,\ N_t = N_b = 0.5, \delta = 0.1, \mathrm{Pr} = 21,\ t = 0.45.$$

FIG. 7. Flow rate profile at different values with the following data $\mathrm{Gr}_N = 3, \delta = 0.1, Pr = 21.$

FIG. 8. Flow rate profile at different values with the following data $\mathrm{Gr}_T = 2, \delta = 0.1, Pr = 21.$

FIG. 9. Wall Shear Stress profile at different values with the following data $\delta = 0.1, Pr = 21.$

FIG. 10. Resistance to flow or impedance at different parameters with the following data

$$\delta = 0.1, Pr = 21.$$

FIG. 11. Streamline of blood flow in artery with the following data $N_t = N_b = 0.5, t = 0.45.$

FIGURES

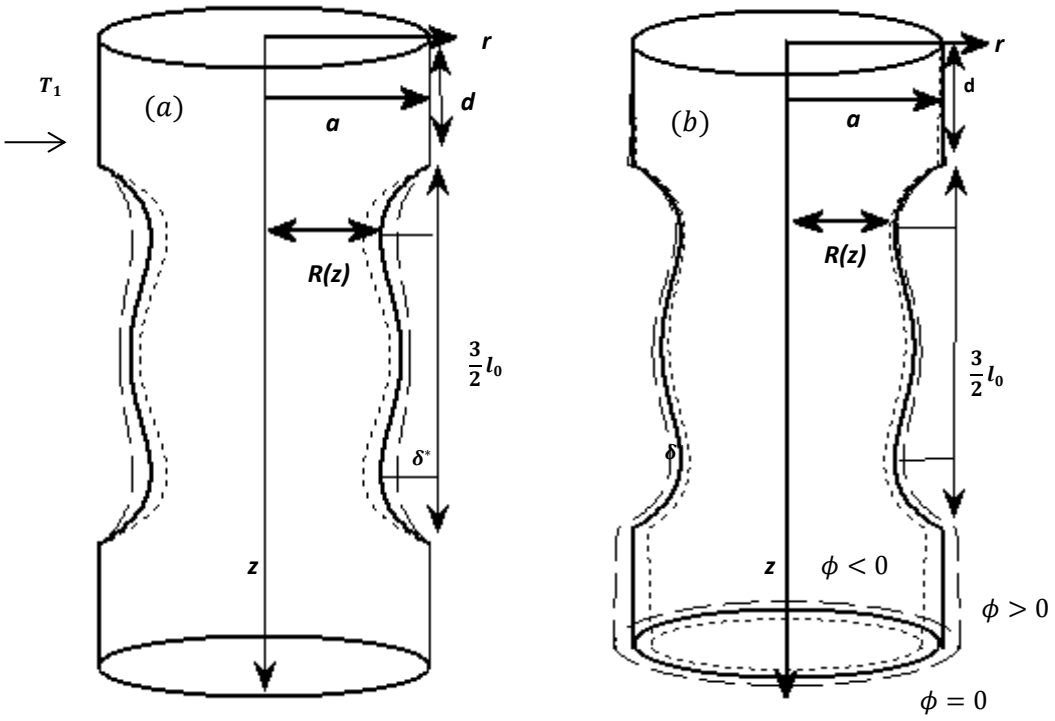

Figure 1: Geometry of the overlapping stenotic artery

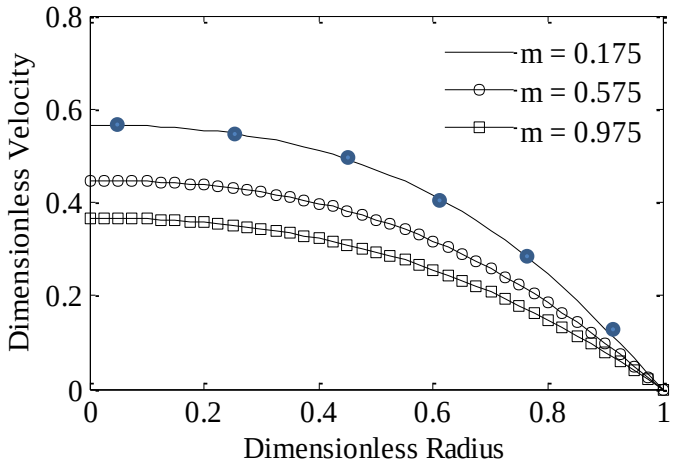

Figure 2. Variation of axial velocity for different values of *m* with

$\mathrm{Gr}_T = 2,\ \mathrm{Gr}_N = 2,\ N_t = N_b = 0.5, Pr = 21,\ t = 0.45.$

(N.B. FEM solutions correspond to blue dot in Figs 2-10)

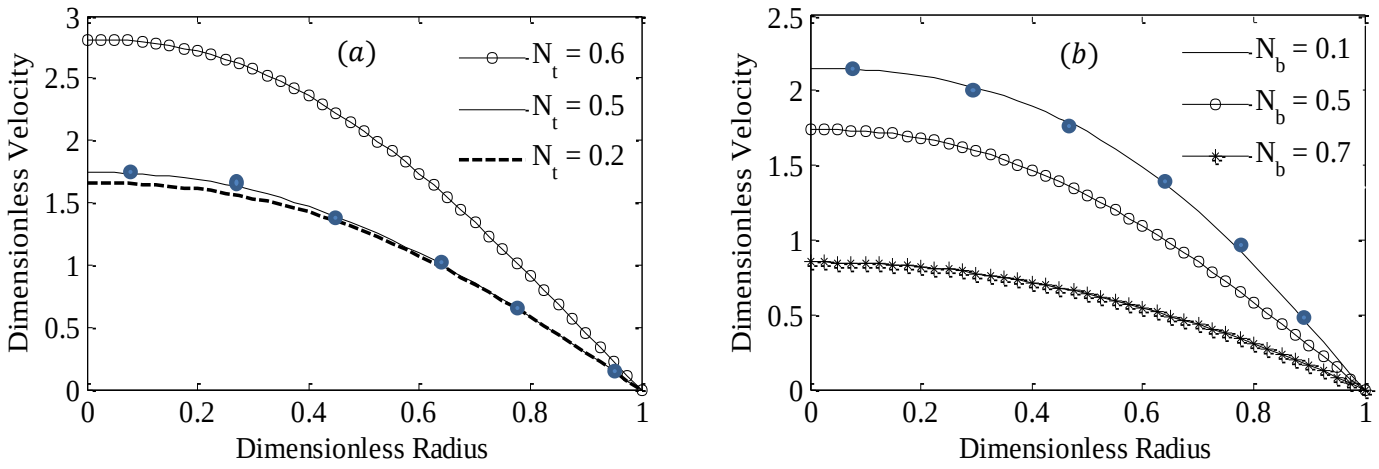

Figure 3. Variation of axial velocity for different values of N_t (left) and N_b (right) with:

$\mathrm{Gr}_T = 2,\ \mathrm{Gr}_N = 2,\ N_t = N_b = 0.5, Pr = 21,\ t = 0.45.$

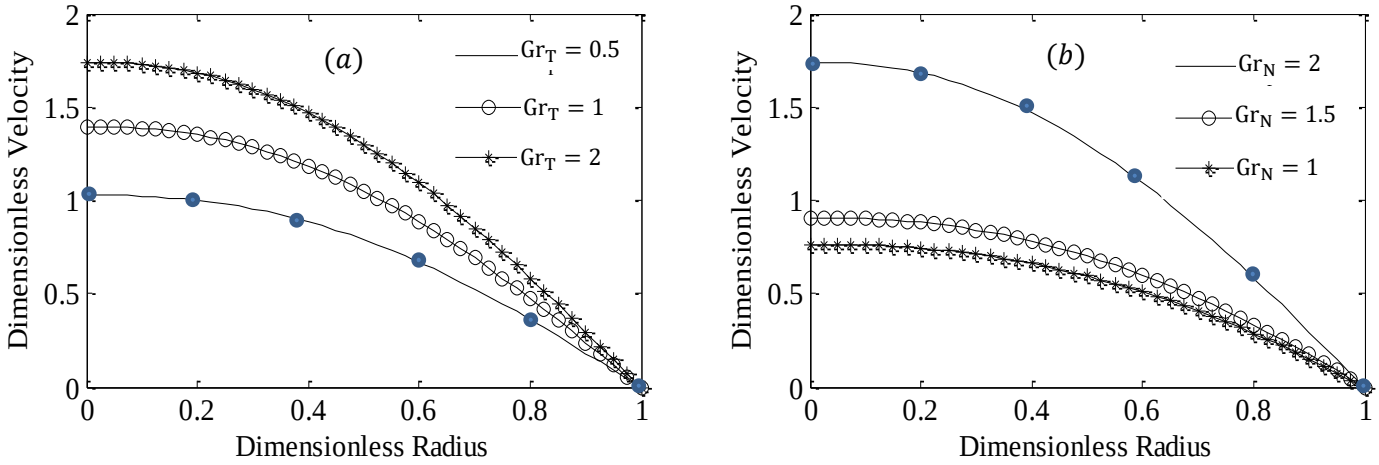

Figure 4 (a). Variation of axial velocity for different values of Gr_T with the following data*:*

$N_t = N_b = 0.5,\ m = 0.175, \delta = 0.1,\ \mathrm{Pr} = 21,\ \mathrm{Gr}_T = 2,\ t = 0.45.$

Figure 4 (b). Variation of axial velocity for different values of Gr_N with the following data*:*

$N_t = N_b = 0.5,\ m = 0.175, \delta = 0.1,\ \mathrm{Pr} = 21,\ \mathrm{Gr}_N = 2,\ t = 0.45.$

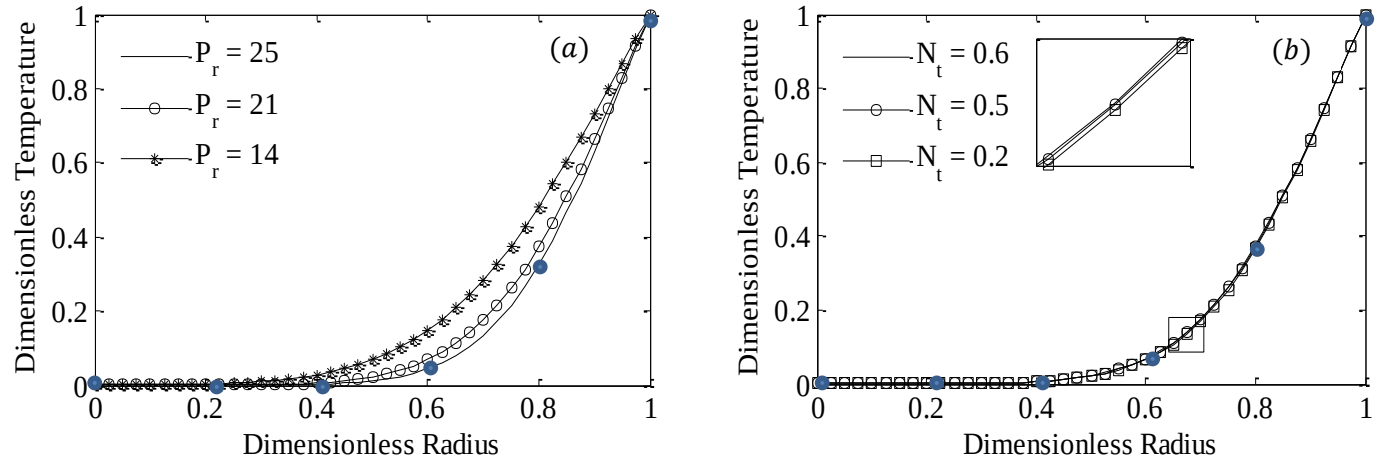

Figure 5 (a). Temperature profile at different values of P_r with the following data*:*

$\mathrm{Gr}_T = 2,\ \mathrm{Gr}_N = 2,\ N_t = 0.5, \delta = 0.1, t = 0.45.$

Figure 5 (b). Temperature profile at different values of N_t with the following data*:*

$\mathrm{Gr}_T = 2,\ \mathrm{Gr}_N = 2,\ Pr = 21, \delta = 0.1,\ t = 0.45.$

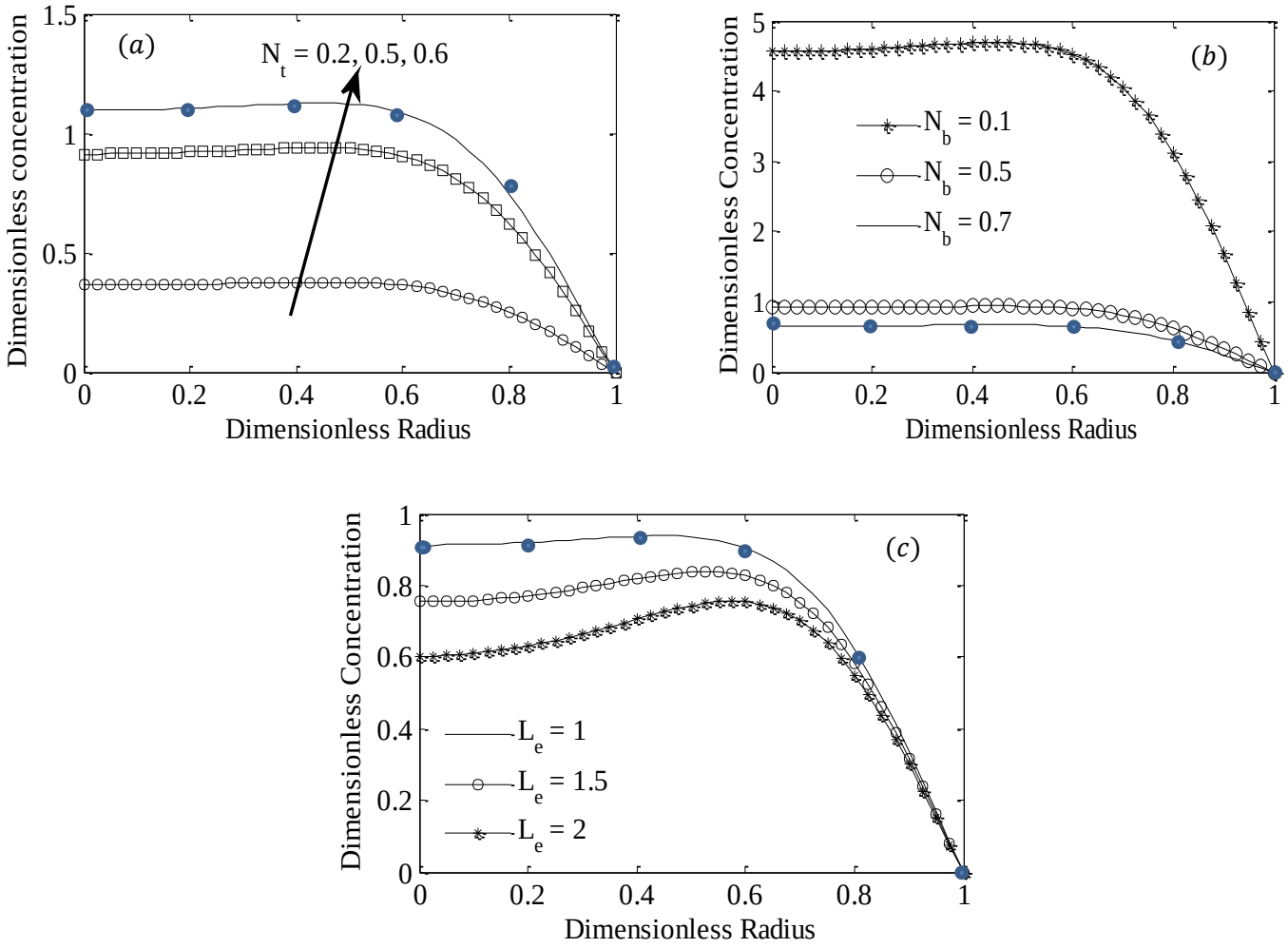

Figure 6(a). Concentration of mas profile at different values of N_t with the following data*:*

$$\mathrm{Gr}_T = 2,\ \mathrm{Gr}_N = 2,\ Le = 1,\ N_b = 0.5, \delta = 0.1, \mathrm{Pr} = 21,\ t = 0.45.$$

Figure 6 (b). Concentration of mas profile at different values of N_b with the following data*:*

$$\mathrm{Gr}_T = 2,\ \mathrm{Gr}_N = 2,\ N_t = 0.5, Le = 1, \delta = 0.1, \mathrm{Pr} = 21,\ t = 0.45.$$

Figure 6 (c). Concentration of mas profile at different values of *Le* with the following data*:*

$$\mathrm{Gr}_T = 2,\ \mathrm{Gr}_N = 2,\ N_t = N_b = 0.5, \delta = 0.1, \mathrm{Pr} = 21,\ t = 0.45.$$

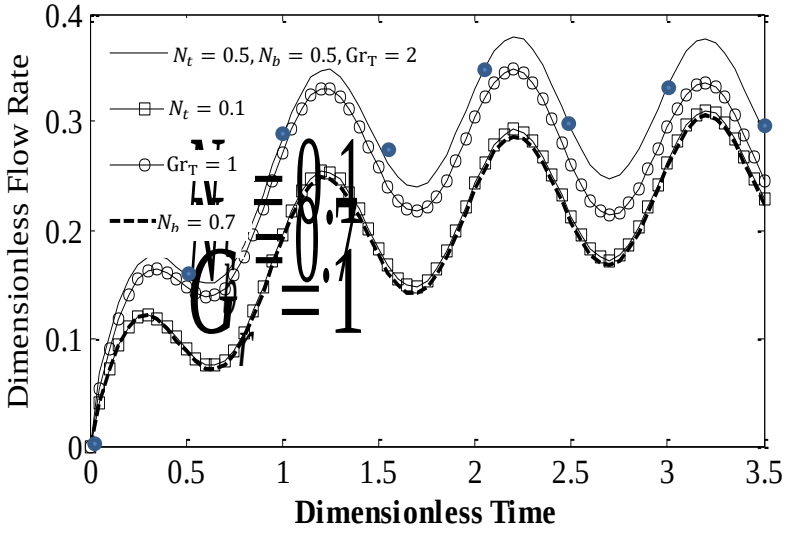

Figure 7. Flow rate profile at different values with the following data $\mathrm{Gr}_N = 3, \delta = 0.1, Pr = 21.$

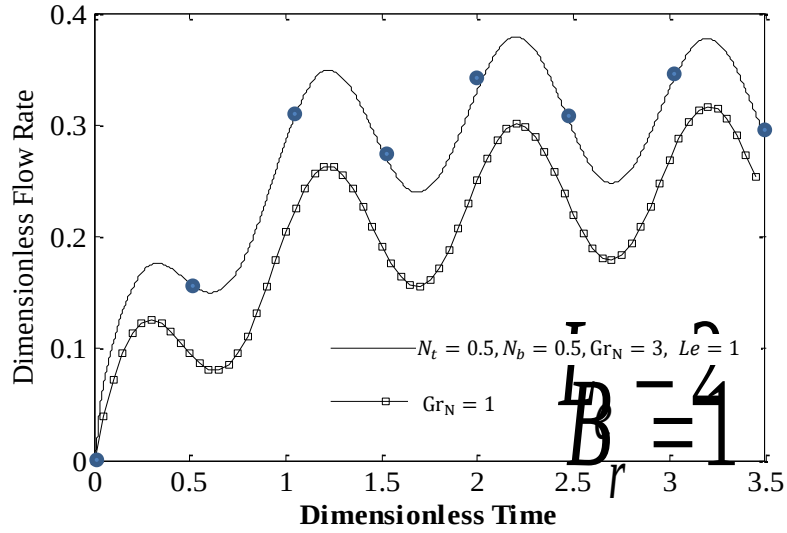

Figure 8. Flow rate profile at different values with the following data $\mathrm{Gr}_T = 2, \delta = 0.1, Pr = 21.$

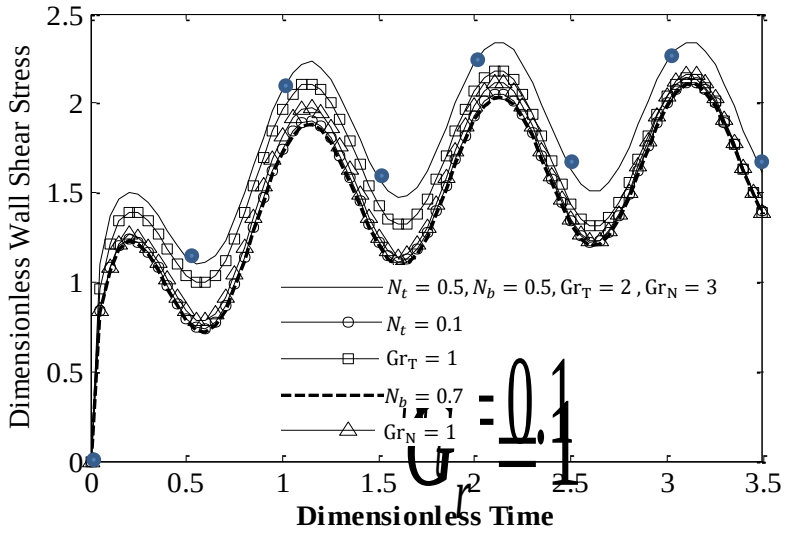

Fig. 9. Wall Shear Stress profile at different values with the following data $\delta = 0.1, Pr = 21.$

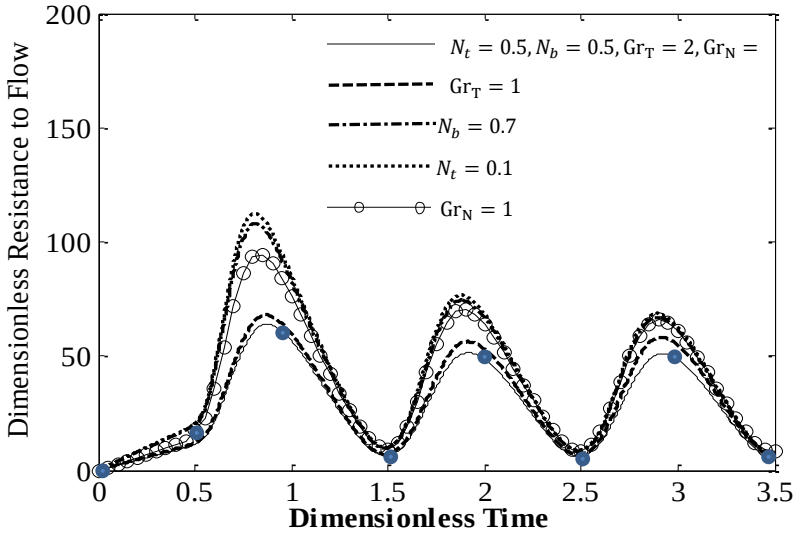

Figure 10. Resistance to flow or impedance at different parameters with the following data*:* $\delta = 0.1, Pr = 21.$

.

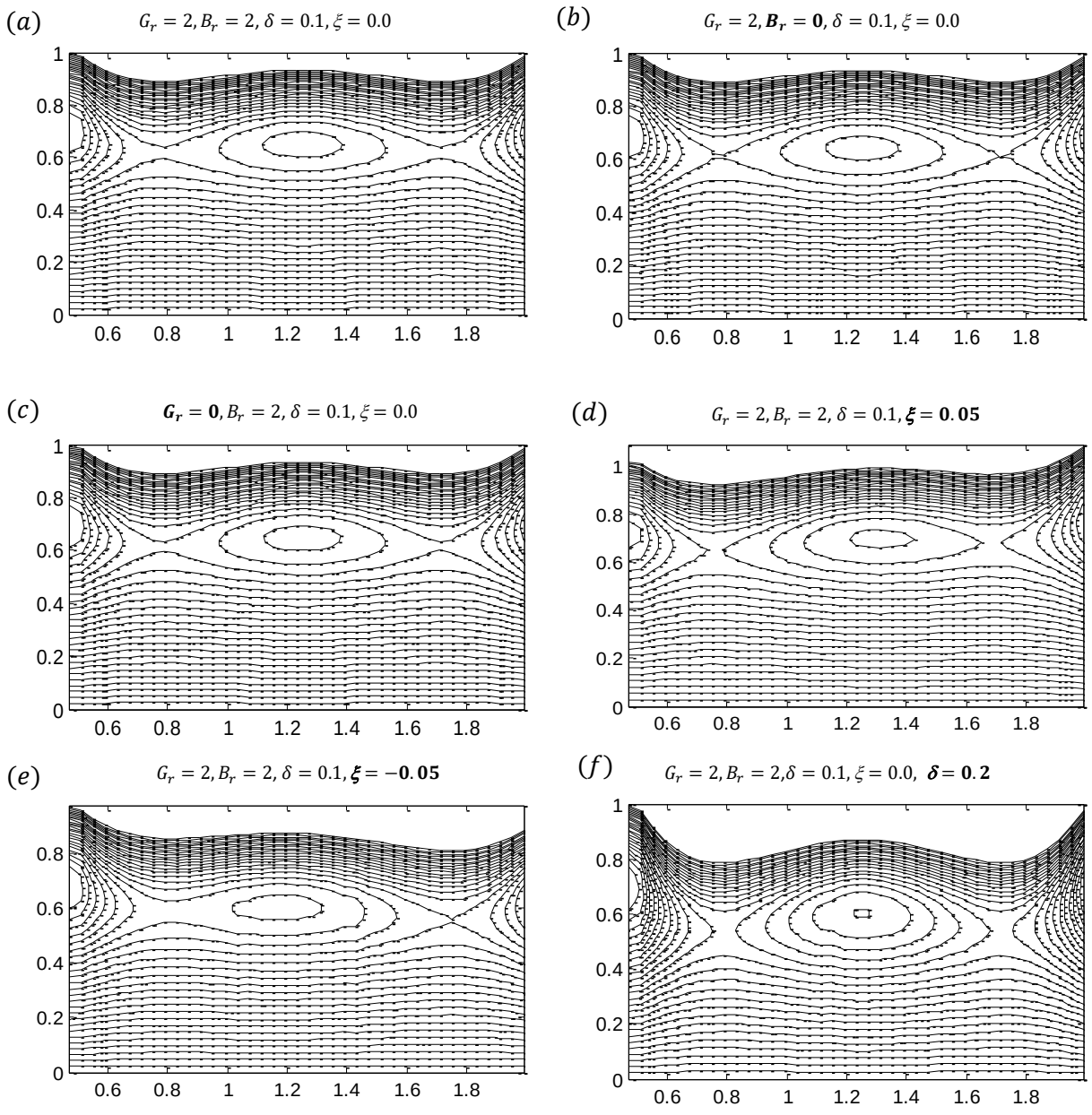

Figure 11. Streamline of blood flow in artery with the following data*:* $N_t = N_b = 0.5, t = 0.45.$